Available online at www.CivileJournal.org

Civil Engineering Journal

(E-ISSN: 2476-3055; ISSN: 2676-6957)

Vol. 11, No. 12, December, 2025

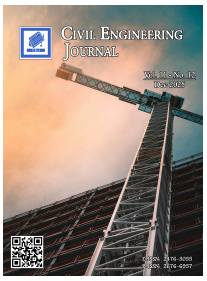

Influence of Polypropylene Fiber on Mechanical and Shrinkage Behavior of Porcelain Based Geopolymer

Rada Klingsad [1], Borvorn Israngkura Na Ayudhya [1*]

[1] *Department of Civil Engineering, Faculty of Engineering, Rajamangala University of Technology Thanyaburi, Pathum Thani 12110, Thailand.*

Received 01 September 2025; Revised 17 November 2025; Accepted 22 November 2025; Published 01 December 2025

Abstract

This study examines the effects of polypropylene (PP) fiber content and initial curing temperature on shrinkages, mechanical properties, and microstructural characteristics of porcelain-based geopolymers. Geopolymer mixes were prepared with PP fiber dosages of 0.5%, 1.0%, 1.5%, and 2.0% by weight and initially cured at 60 °C, 75 °C, 90 °C, and 105 °C. Autogenous and drying shrinkage were monitored at 24 h, 72 h and 3, 7, 14, 21, 28, 60, 90, and 120 days, while compressive and splitting tensile strengths were tested at 3, 7, 14, 21, and 28 days. The results demonstrated that the incorporation of PP fiber not only shortened the setting time but also significantly reduced both autogenous and drying shrinkage of the geopolymer mortar. The most favorable performance was observed in specimens containing 2.0% PP fiber cured at 105 °C, which exhibited the lowest shrinkage values. Autogenous shrinkage was 439 $\mu\varepsilon$ at 24 h and 392 $\mu\varepsilon$ at 120 days, while drying shrinkage was 544 $\mu\varepsilon$ at 24 h and 194 $\mu\varepsilon$ at 120 days. Increasing fiber content decreased porosity, producing a more compact, homogeneous matrix and improving mechanical performance of concrete specimens, particularly splitting tensile strength; the optimal dosage was 2%, yielding 28-day compressive strength of 41.03 N/mm² and splitting tensile strength of 7.65 N/mm².

Keywords: Geopolymers; Drying Shrinkage; Augenous Shirnkage; Porcelain; Splitting Tensile.

1. Introduction

Geopolymers are an innovative and eco-friendly alternative to Ordinary Portland Cement (OPC), significantly reducing carbon emissions because their production does not involve the high-temperature calcination process used in cement production, which is a major source of energy consumption and carbon emissions. Instead, the geopolymerization process involves the chemical reaction of aluminosilicate materials in an alkaline environment to form a hardened, cement-like material. Cement production requires 110-120 kWh of electrical energy per one ton of cement [1]. Thermal energy is mainly used during the burning process, while electrical energy is consumed during the grinding process. Geopolymers not only offer substantial reductions in carbon emissions but also provide superior mechanical strength and durability performance, promoting sustainable construction practices globally [2]. Geopolymers require supplementary cementitious materials as binders. Introducing industrial waste materials such as fly ash, slag, and other by-products can be utilized as geopolymer binders, which helps in reducing waste and promoting sustainable resource management. Porcelain is a strong and durable ceramic material. It is made from a combination of fine-grained clays and other raw materials like kaolin, feldspar, and quartz. High firing temperatures (1,200°C to 1,400°C) produce a non-porous, glassy structure, which gives porcelain its characteristic hardness and scratch resistance. Despite its high hardness, porcelain remains brittle and fragile. Advanced methods are being developed to minimize

* Corresponding author: borvorn_i@rmutt.ac.th

http://dx.doi.org/10.28991/CEJ-2025-011-12-024

defects in porcelain manufacturing, since defective products, which account for 3-5% of total production, are typically landfilled. Porcelain is a low-calcium material. The primary material used in producing porcelain is low calcium content. The low-calcium feedstocks contribute to unique geopolymer concrete properties such as high compressive strength, low creep [3], and excellent resistance to sulfates and acids [4]. These characteristics make low-calcium geopolymer concrete highly suitable for infrastructure applications.

To enhance strength and toughness, natural and synthetic fibers are commonly used. Various studies have highlighted the advantages of adding fibers such as basalt [5], flax [6], polyvinyl alcohol (PVA) [7], and polypropylene (PP) [8] to improve specimen properties. Polymer-based fibers are preferred because of their superior chemical resistance and durability. Specifically, PP fibers offer long-term degradability, minimize spalling, improve early-age crack resistance [9-11], and reduce maintenance costs, making PP fibers ideal for environments prone to severe chemical corrosion. Zhang et al. [12] demonstrated that incorporating PP fibers into low-calcium fly ash increased flexural strength by 39% compared to non-fiber specimens. Gholampour et al. [13] reported a 123% rise in compressive strength in slag-based geopolymer specimens with 1% PP fiber inclusion, although this also led to a 15% increase in drying shrinkage. Hong et al. [14] demonstrated that adding 0.3% PVA fiber reduced shrinkage in low-calcium fly ash geopolymer mortar. Panti & Patil [15] showed that varying the proportions and widths of PP fiber improved the splitting tensile strength of low-calcium fly ash geopolymer concrete, achieving a maximum 12.2% increase over control specimens. Hongen et al. [16] observed that using 0.5% steel and polypropylene fibers minimized stress distribution and crack mouth opening displacement in low-calcium fly ash concrete. Additionally, Rios et al. [17] stated the micro-PP fiber with a length of 24 mm exhibited greater fracture energy compared to shorter fibers in low-calcium fly ash formulations.

Shrinkage is a key factor influencing the durability and long-term performance of low-calcium geopolymer concrete. While this sustainable material offers numerous advantages over traditional Portland cement concrete, effectively managing shrinkage is crucial for its broader adoption in construction. Dry shrinkage results from moisture loss over time, leading to contraction and micro-crack formation, particularly in restrained specimens. Fibers are commonly used to mitigate cracks in mortar and concrete. Synthetic fiber, such as PP, can reduce shrinkage to varying degrees. In order to mitigate drying shrinkage in geopolymer concrete and enhance performance and durability, researchers have identified the key issues and organized them into five aspects for consideration: (1) Optimizing mix design by lowering the water-to-solid ratio or reducing water in the alkaline activator decreases drying shrinkage by minimizing evaporative loss. This approach reduces the water content and helps minimize water evaporation, which is a primary cause of drying shrinkage. Peng et al. [18] reported that an increase in the liquid–solid ratio had minimal effect on capillary pore distribution but significantly deteriorated shrinkage resistance properties of the paste, leading to increased drying shrinkage. Hanumananaik et al. [19] found that drying shrinkage depends on the water and sodium contents in the activated paste. (2) Incorporating fibers and additives, PP fibers strengthen internal bonding and limit shrinkage-induced cracking. It enhances internal bonding and reduces crack propagation caused by shrinkage. Huang et al. [20] demonstrated that fibers inhibited shrinkage in low-calcium geopolymer mortar.

Chen et al. [21] found that short fibers significantly decreased the dry shrinkage rates in binary binding material-based geopolymer mortar. (3) Refining curing conditions; maintaining proper humidity and temperature during curing prevents excessive drying. Shamsah et al. [22] reported that curing at 70°C increased compressive strength by 15% in 6M and 8M mixtures compared to ambient curing. Wu et al. [23] found that steam curing accelerated polymerization reactions, improving early strength development in FA-OPC-SF-based geopolymer mortar. (4) Optimizing alkali activator concentration: Selecting the right molar concentration ensures a denser, shrinkage-resistant matrix. Alkali concentration effects: the molar concentration of the alkali solution (commonly sodium hydroxide, NaOH, or potassium hydroxide, KOH) significantly impacts the drying shrinkage behavior of geopolymer concrete. Trincal et al. [24] found that sodium silicate-activated metakaolin exhibited greater autogenous deformation than desiccation shrinkage, which depended on the environmental conditions and the measurement methods. Ilcan et al. [25] reported that 4M NaOH concentration was inadequate for early strength development in construction demolition waste-based geopolymer mortar, regardless of the precursor content. However, using a lower molar concentration caused incomplete polymerization; a weaker alkali solution results in less efficient geopolymerization, leaving parts of the matrix susceptible to shrinkage [26]. (5) Utilizing supplementary materials. Low-calcium materials such as fly ash type F and slag improve workability and reduce shrinkage through geopolymerization. De Klerk et al. [27] reported that combining 20% fly ash type F with 40% GGBS significantly lowered drying shrinkage to below 0.5%. Yan et al. [28] found ternary mixes of slag, fly ash type F, and ceramic waste powder exhibited shrinkage rates 1.5-2.0 times lower than standard geopolymer concrete.

While previous research studies have explored the effects of low calcium binders (fly ash, GGBS, and metakaolin) on natural and synthetic fiber-reinforced specimens [29-30]. The available data on porcelain-based geopolymers reinforced with PP fiber remain limited. Low-calcium-material-based geopolymers have been shown to have lower drying shrinkage and creep. Porcelain waste as low-calcium precursors is underexplored. This was due to the long-time preparation of the porcelain powder process, which required several stages of producing

porcelain powder (hammering, chopping, cutting, grinding, milling, and sieving). This study extends knowledge on the linkage between early-age and long-term performance that correlates microstructure evolution with mechanical and shrinkage behavior of PP in defective sanitary ware porcelain powder-based geopolymer composites. It also addresses the understanding of dosage–temperature interactions: systematic studies combining various PP fiber contents with different initial curing temperatures. The study also examines the limits of workability for practical PP dosages and investigates how mix design can be optimized to balance fresh-state rheology with hardened-state properties. The insights gained from this study provide a foundational understanding of key properties, supporting the use of porcelain and PP fiber in developing effective geopolymer composite matrices for various applications. The porcelain waste powder used in this research originates from defective sanitary ware products and is repurposed as cementitious material, undergoing geopolymerization using an alkaline solution of NaOH and Na_2SiO_3. Importantly, this low calcium binder material is neither thermally nor chemically activated. The structure of this study was shown in Figure 1.

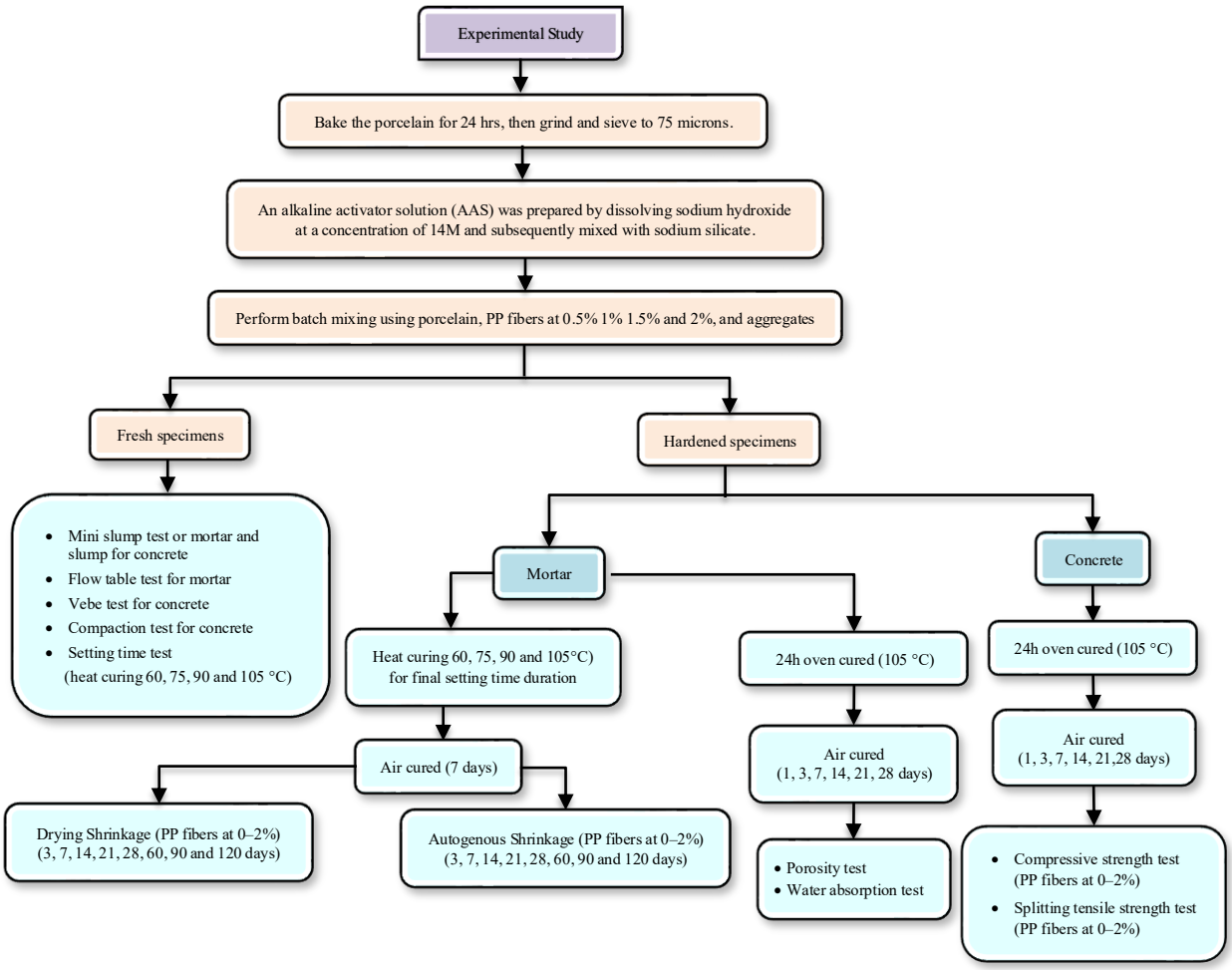

Figure 1. Schematic flow of research

2. Materials

2.1. Cementitious Materials and Fiber

2.1.1. Porcelain Powder

The geopolymer binder was prepared by mixing porcelain powder (as shown in Figure 2) with an alkaline activator solution at a mass ratio of 1:1.43. The alkali-activated solution (AAS) itself was prepared with a solution-to-binder ratio of 2.5. The chemical composition of the porcelain powder was analyzed by using X-ray fluorescence (XRF). The result was presented and compared with high- and low-calcium materials (Table 1). The XRF analysis was conducted by using a Bruker S8 Tiger spectrometer under vacuum conditions. To determine the particle size distribution, a laser particle size analyzer (Malvern Mastersizer 3000) was employed. The characterization revealed that the porcelain powder is predominantly composed of silica (SiO_2) and alumina (Al_2O_3), with relatively low calcium oxide (CaO) content. This composition supports its suitability as a low-calcium precursor for geopolymer synthesis.

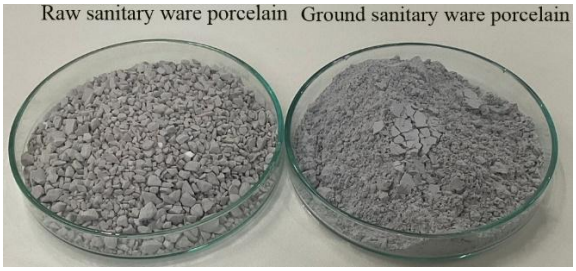

Figure 2. Raw material before and after ground porcelain material

Table 1. Chemical analysis and physical properties of defected sanitary porcelain and OPC material

Oxides	Porcelain (%)	GGBFS [31]	Fly ash (Type F) [32]	Steel Slag [33]
CaO	2.68	41.83	4.75	36.10
SiO_2	56.21	33.08	52.90	17.96
Al_2O_3	18.23	14.99	25.50	6.93
SO_3	0.03	2.28	2.90	0.77
Fe_2O_3	1.67	0.63	8.70	22.04
MgO	0.41	5.92	3.10	8.22
K_2O	3.12	0.31	2.00	0.47
TiO_2	0.20	0.55	-	0.95
Na_2O	1.14	0	0.15	-
Others	8.09	0.09	-	-
LOI	8.22	0.32	0.53	-
Particle size				
D_{10}	2.22			
D_{50}	16.7			
D_{90}	52.4			

The average particle size (D_{50}) of the porcelain powder used in this study was measured to be 52.4 µm. The alkaline activator solution (AAS) was composed of sodium hydroxide (NaOH) and sodium silicate ($Na_2O{\cdot}2SiO_2$). Sodium hydroxide solutions with concentrations of 14M were prepared by using analytical-grade NaOH flakes (>99% purity). The commercial sodium silicate solution contained 63.4% H_2O, 24.7% SiO_2, and 11.9% Na_2O by weight. In the first stage of preparation, NaOH flakes were dissolved in deionized water to achieve the desired molar concentrations. These solutions were allowed to cool down at room temperature before solutions were mixed with sodium silicate to form the final alkali-activated solution. The exothermic reaction during mixing was allowed to dissipate naturally. Once the AAS was stabilized, additional water and a superplasticizer (SP) were added to enhance the workability of the fresh porcelain-based geopolymer mix. A polycarboxylate-based superplasticizer was used at a dosage of 1% by weight of porcelain powder.

2.1.2. Polypropylene (PP) Fiber

The polypropylene (PP) fibers used in this study were incorporated into the mixtures, calculated based on the geopolymer concrete volume. Figure 3 displays the PP fibers utilized in the experimental program. Table 2 summarizes their key physical properties.

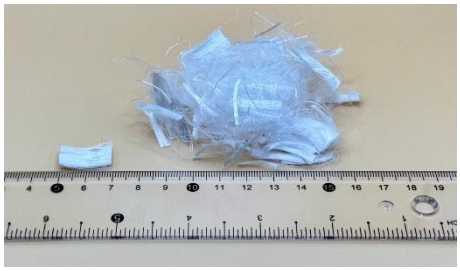

Figure 3. Polypropylene fiber

Table 2. Basic properties of PP fiber

Properties	Data
Specific gravity (g/cm^3)	0.91
Tensile strength (N/mm^2)	300-400
Modulus of Elasticity (KN/mm^2)	8000
Elongation at yield (%)	13
Water absorption	Nil
Range of melting temperature (°C)	160-175
Evaporation point (°C)	341
Burning temperature (°C)	460

3. Experimental Methods

3.1. Mixture and Specimen Preparations

Three different mix types (paste, mortar, and concrete) were prepared for this study. Figure 3 illustrated overview of the experimental workflow for this study while Table 3 presented the specific mixture proportions used for each specimen. For geopolymer paste preparation, geopolymer paste was cast into conical molds with dimensions of 40 mm. depth, 80 mm. top diameter, and 100 mm. bottom diameter. Porcelain powder was mixed with alkali-activated solutions (14M) using a planetary mixer for 2 min. PP fiber was then added and the mixture was stirred for an additional 3 min. before ready-mix was cast into molds. For geopolymer mortar preparation, all mortar mixes, a sand-to-binder ratio of 0.863 was maintained. Initial curing was conducted at temperatures of 60 °C, 75 °C, 90 °C, and 105 °C for 2 h. followed by air curing for 3, 7, 14, 21 and 28 days. The curing regimes (60 °C-105 °C) adopted in this study were based on findings from previous investigations [34-36]. To prepare fiber-reinforced geopolymer mortar specimens: dry materials (porcelain powder and fine aggregate) were mixed for 2 min. Then alkali activator solution was added and mixed for 3 min. PP fiber was introduced and mixed for an additional 2 min. Fresh mortar was placed into pre-oiled steel molds (25 × 25 × 280 mm.^{3}) equipped with studs at both ends and a steel upper plate to prevent expansion. Mortar specimens were demolded after 2 h. of curing in a drying oven at 105 °C. For autogenous shrinkage testing, specimens were wrapped in two layers: an inner layer was polypropylene film and an outer layer was aluminum foil sheet.

Table 3. Mixture proportion of paste, mortar and concrete specimens

Paste										
Code	NaOH (M)	Solid content (%)	AAS Ratio	Materials (kg/m^3)						
				NaOH	Na_2SiO_3	Porcelain	Fine aggregate	SP	PP Fiber (%)	Curing temperature (°C)
P-GPC14	14	52.5	2.5	100	250	500	-	5	0.5, 1.0, 1.5 and 2.0	60, 75, 90, 105
Mortar										
Code	NaOH (M)	Solid content (%)	AAS Ratio	Materials (kg/m^3)						
				NaOH	Na_2SiO_3	Porcelain	Fine aggregate	SP	PP Fiber (%)	Curing temperature (°C)
M-GPC14	14	52.5	2.5	100	250	500	431.34	5	0.5, 1.0, 1.5 and 2.0	60,75, 90, 105
Concrete										
Code	NaOH (M)	Solid content (%)	AAS Ratio	Materials (kg/m^3)						
				NaOH	Na_2SiO_3	Porcelain	Fine aggregate	SP	Coarse aggregate	PP Fiber (%)	Curing temperature (°C)
C-GPC14	14	52.5	2.5	100	250	500	431.34	5	1041.54	0.5, 1.0, 1.5, 2.0	105

For geopolymer concrete preparation, specimens were cast in cylindrical molds (100 × 200 mm.) and cubic molds (50 × 50 × 50 mm). Mixing was conducted under ambient conditions (32 °C ± 2, relative humidity (72%± 5). Preparation steps included dry mixing porcelain powder with aggregates for 2 min. The alkali-activated solution was gradually introduced into the dry mix and mixed for 3 min. to ensure uniform dispersion of the activator throughout the binder matrix. Following this stage, PP fibers were incorporated into the mixture and mixing was continued for an additional 2 min. to achieve homogeneous fiber distribution. Fresh concrete was placed into molds and cured in a drying oven at 105 °C for 24 h. After demolding, specimens were wrapped with polypropylene film and air-cured under ambient conditions for 1, 3, 7, 14, 21, and 28 days.

3.2. Experimental Test Methods

3.2.1. Paste

Immediately after the placing, a setting time test of paste was done based on the procedure described in ASTM C191-13 [37]. The initial setting time was determined when the needle penetrates the paste to a depth of 5.0 ± 0.5 mm. from the top. The final setting time was determined when a circular attachment makes an impression on the paste, indicating complete loss of plasticity. The results of setting time were recorded from the average of three specimens.

3.2.2. Mortar

Porcelain based geopolymer mortars were subjected to drying and autogenous shrinkage tests, the standard protocol in ASTM C596 [38] was applied to measure the drying shrinkage. While, the test method prescribed in ASTM C1698 [39] technique was adopted and modified to measure the autogenous shrinkage. Figure 4 preseted prepared specimens for shrinkage test. The workability of fresh specimens was also observed. In this study, workability was assessed by using both the mini-slump and flow-table tests, as shown in Figure 5. The mini-slump cone used for testing had a height of 60 mm, a top diameter of 36 mm, and bottom diameters of 70 mm. (inner) and 100 mm. (outer) respectively.

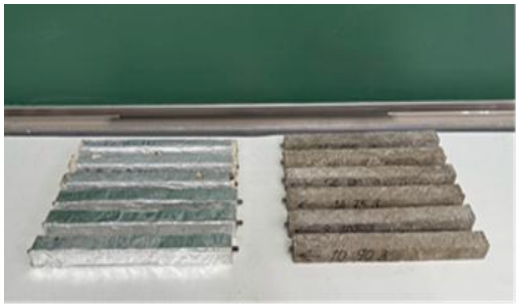

(a) (b)

Figure 4. Prepared specimens for shrinkage tests (a) Autogenous shrinkage specimens (b) drying shrinkage specimens

(a) (b)

Figure 5. Workability of Porcealin based geopolymer with PP fiber mortar (a) Mini-slump (b) Flow-table

3.2.3. Concrete

A microscopic examination of specimens was conducted, focused on their 28-day microstructure using the Field Emission Scanning Electron Microscope and Energy Dispersive X-ray Spectrometer (FESEM-EDS IT800SHL) at 20x magnification. The images provided insight into the microstructure, revealing porcelain particles, fiber orientation, and details of the geopolymer matrix. Fresh porcelain-based geopolymer concrete was tested for workability. Slump flow was measured according to ASTM C143 standard [40]. While, Vebe values were recorded using the BS EN 12350-3-2009 Part 3 technique [41]. For hardened specimens, water absorption and porosity of specimens were measured. Water absorption was determined in accordance with ASTM C642 [42] using 50×50×50 mm. cubical specimens. The porosity test was employed to assess the influence of fiber in the internal pore structure of geopolymer concrete. Since porosity strongly governs strength, permeability, and long-term durability, cube specimens (50 × 50 × 50 mm) were prepared and tested at curing ages of 1, 3, 7, 14, 21, and 28 days. The specimens were placed in a vacuum desiccator for three hours to remove entrapped air, after which distilled water was introduced to fully submerge specimens. The depressurization cycle was repeated to ensure complete saturation, and the saturated masses were recorded. The samples were then oven-dried at 105 °C for 24 h to eliminate residual moisture, and their dry masses were measured under controlled conditions. Porosity was subsequently calculated using Equation 1:

$$Porosity\ (\%) = \left(\frac{m_{a\,(sat)} - m_{a\,(sat)}}{m_{a\,(sat)} - m_{w\,(sat)}}\right) \times 100 \quad (1)$$

where $m_{a\,(sat)}$ = Mass of saturated specimens in air (g), $m_{w\,(sat)}$ = Mass of saturated specimen in water (g), and $m_{a\,(dry)}$ = Mass of oven dried specimens in air (g).

Cylindrical specimens of 100×200 mm. prisms were used for both compressive and splitting tensile tests. The compressive strength of porcelain based geopolymer concretes was carried out according to ASTM C109/C109M-16a [43]. While, the splitting tensile strength was tested in accordance with ASTM C496-96 [44]. The results were reported from the average of three specimens. All concrete specimens were oven-dried for 24 h at 105 °C before being air-cured for 3, 7, 14, 21, and 28 days.

4. Results and Discussion

4.1. Setting Time and Flow Ability

Figure 6 illustrated the variation in setting time of porcelain-based geopolymer paste as a function of PP fiber content. Initial and final setting times for mixes containing 0.5%, 1.0%, 1.5%, and 2.0% PP fiber were presented in Table 4. The shortest initial and longest final setting times were recorded at 91 min. and 692 min. respectively. Considering fiber content effect to setting time, the study found that increasing the amout of PP fiber in the mix contributed to a reduction in setting time. Both initial and final setting times increased when PP fiber content decreased. This trend contrasts with previous studies involving high-calcium fly ash geopolymer systems. Pangdaeng et al. [45] reported rapid setting in low-calcium fly ash based geopolymers mixed with PVA and PP fibers, while Punurai et al. [46] observed similar behavior in low calcium fly ash geopolymers reinforced with basalt fibers. In the present study, fast setting was not found in porcelain-based geopolymer mortars containing PP fiber on low (60 °C and 70 °C) initial curing temperature (Figures 6-a and 6-b). This discrepancy may be attributed to the finer particle size and lower specific surface area of porcelain powder compared to fly ash, which slows the geopolymerization reaction.

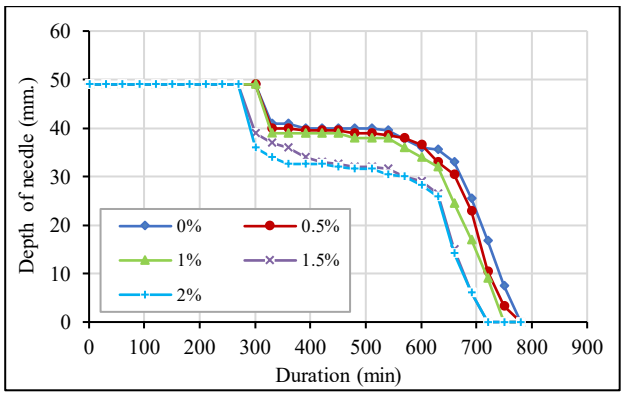

(a) Specimens cured with 60°C

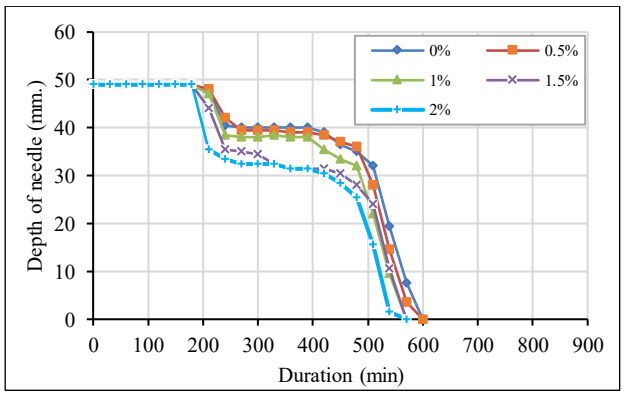

(b) Specimens cured with 75°C

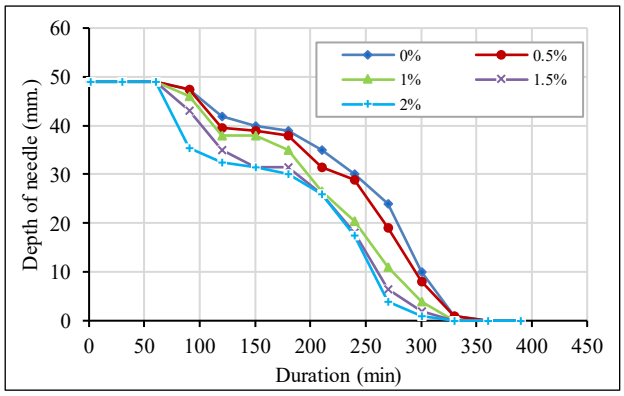

(c) Specimens cured with 90 °C

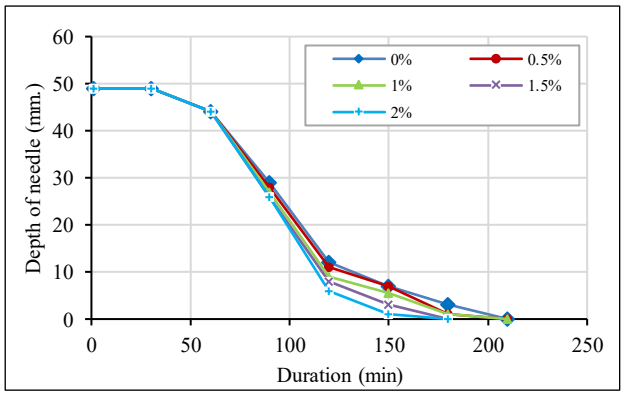

(d) Specimens cured with 105 °C

Figure 6. Charecteristic of porcelain based geopolymer paste with PP fiber on setting

In contrast, when specimens were cured at elevated temperatures of 90°C and 105°C, a significantly rapid setting was noticed, with specimens hardening within 60 min. and 30 min., respectively (Figures 6-c and 6-d). At low temperatures, the onset of hardening was slower, beginning only after 270 min. and 180 min., respectively. Additionally, the study also found that a 14M sodium hydroxide concentration led to high viscosity in the mix, resulting in a reduction in flowability. High concentrations of sodium hydroxide solution were found to prolong setting time. This was due to slower reaction kinetics. The result concurred with the findings of Lee & Lee [47]. This observation also aligns with Guo et al.'s study [48]. He reported that fiber content significantly influences the setting and hardening behavior of geopolymer matrices. This decline in setting time was primarily attributed to the stabilizing effect of PP fiber, which helped maintain mix uniformity and prevent segregation. However, the incorporation of alkaline solutions, water, and

superplasticizers was shown to enhance both the flowability and the cohesiveness of the binder system. Sodium hydroxide plays a key role in regulating the viscosity of sodium silicate, thereby improving mix fluidity [49]. Hannawi et al.'s [50] findings support this trend, showing a linear decrease in workability and setting time with increasing NaOH concentration in porcelain-based geopolymer concrete. These results highlight the complex interplay between fiber content, alkali concentration, and binder composition in determining the fresh and hardened properties of geopolymer mortars. Table 4 presented the workability results for geopolymer mortar mixes containing PP fiber. Both mini-slump and flowability measurements showed a decline as fiber dosage increased, indicating a reduction in overall workability. This decrease is mainly attributed to the greater surface area and volume introduced by the fibers, which heighten shear friction between the fibers and the surrounding matrix [48]. Despite this, the inclusion of fibers also helped minimize segregation, promoting a more homogeneous mix. A sharp drop in workability was noticed when fiber content increased from 0.5% to 1.0%, resulting in a 38% reduction in flowability and a 35% decrease in mini-slump. Consequently, the use of superplasticizers became essential to maintain both workability and mechanical performance when fiber content exceeded 0.5%.

Table 4. Setting time and workability of porcelain based geopolymer paste mixed with PP fiber

	Setting time (min.)								Mini slump (mm.)	Flow-table (%)
	Initial				Final					
PP%	60 °C	75 °C	90 °C	105 °C	60 °C	75 °C	90 °C	105 °C	33 °C ± 2 (Room temperature)	
0	692	527	265	97	780	600	360	210	43	105
0.5	681	516	252	95	780	600	360	210	43	103
1.0	658	502	217	93	750	570	330	210	28	65
1.5	634	501	214	92	720	570	330	180	22	54
2.0	632	481	213	91	720	570	330	180	16	39

4.2. Microstructure

Figures 7-a to 7-d presented scanning electron microscopy (SEM) micrographs of porcelain-based geopolymer concrete specimens reinforced with PP fibers. The specimens were collected following compressive strength testing and reveal a randomly oriented fiber distribution within the matrix. It found that PP fiber was not uniformly dispersed; localized fiber agglomerations occurred in certain zones. The smooth surface texture of the PP fiber facilitated their integration into the matrix, contributing to improved distribution and bonding.

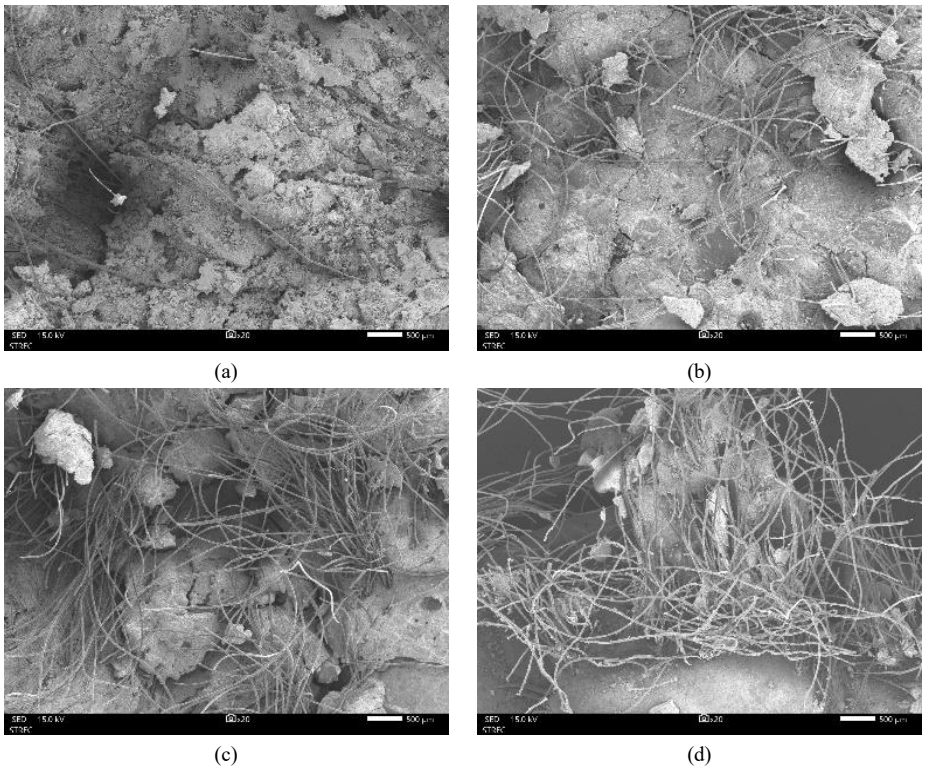

(a) (b) (c) (d)

Figure 7. A 20X magnification of porcelain based geopolymer concrete at 28 days curing time. (a) 0.5% fiber specimens (b) 1.0X% fiber specimens (c) 1.5% fiber specimens (d) 2.0% fiber specimens

As fiber content increased, the SEM images showed a noticeable reduction in microcracks, which correlates with the observed enhancements in compressive and splitting tensile strength, as well as reductions in water absorption and shrinkage. The improved bonding between PP fiber and the geopolymer matrix at higher fiber dosages contributed to a more cohesive and durable structure. These findings are consistent with the results reported by Hannawi et al. [50], who observed that increasing fiber content led to a denser microstructure with fewer crack lines, reinforcing the role of fiber reinforcement in enhancing the mechanical and durability properties of geopolymer composites.

4.3. Shrinkages

4.3.1. The effect of Fiber Content

To assess the influence of PP fiber content on the shrinkage behavior of porcelain-based geopolymer mortar, both autogenous and drying shrinkage were monitored over multiple time intervals—initial 72 hours and at 3, 7, 14, 21, 28, 60, 90, and 120 days. Mortar specimens were cast in standard molds of dimension $2.5 \times 2.5 \times 28.5$ cm³. As shown in Figure 8, increasing PP fiber content led to a reduction in autogenous shrinkage. A similar trend was found in drying shrinkage, although the reduction was less significant. This discrepancy was likely influenced by environmental factors such as ambient humidity and exposure during the drying process. All mixes used an activating solution with a 14M alkali concentration.

Figures 8-a to 8-d presented the drying shrinkage of porcelain-based geopolymer mortars with varying PP fiber contents over a period of 72h. The results revealed distinct shrinkage behaviors across varying PP fiber contents and initial curing temperatures, underscoring the combined influence of fiber reinforcement and thermal curing on the dimensional stability of geopolymer concrete. Both drying and autogenous shrinkage rates rose sharply within the first 24 h. During 24 h, the autogenous shrinkage of porcelain based geopolymer mortars fell in a broad range from 388με to 524με. The lowest autogenous shrinkage was found to be specimen mixed with 2% fiber content and treated with curing temperature of 60°C; whereas, the specimens mixed with 0% PP fiber and treated with curing temperature of 105°C was found to be the highest autogenous shrinkage. Compared with previous studies which have reported that cement paste with a water-to-cement ratio of 0.40 typically exhibits autogenous shrinkage around 130 με [51].

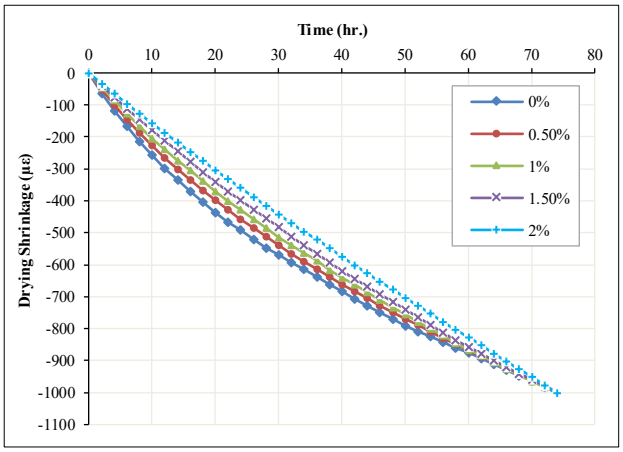

(a) Drying shrinkage of specimen after curing at 60°C

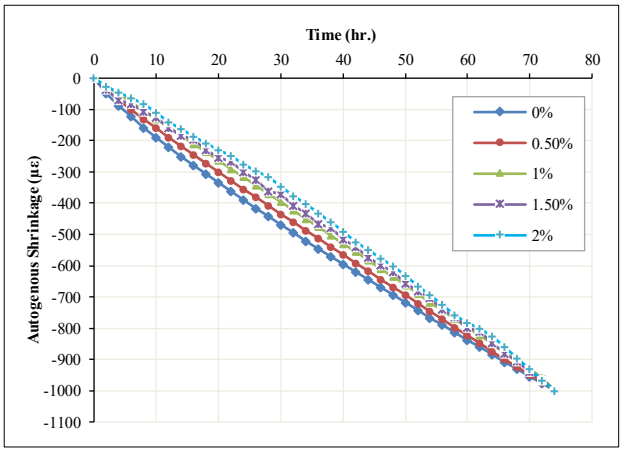

(b) Autogenous shrinkage of specimen after curing at 60°C

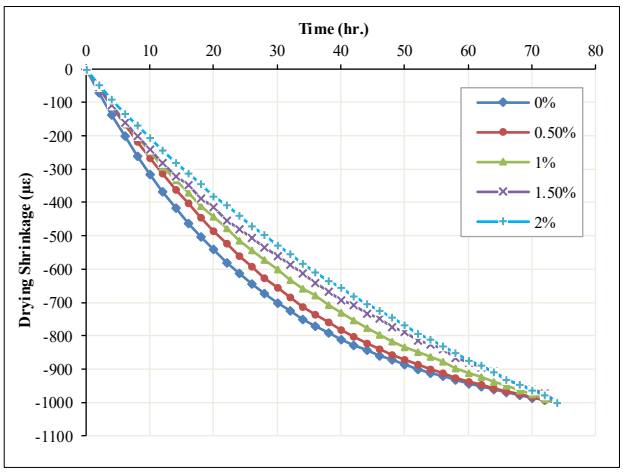

(c) Drying shrinkage of specimen after curing at 105°C

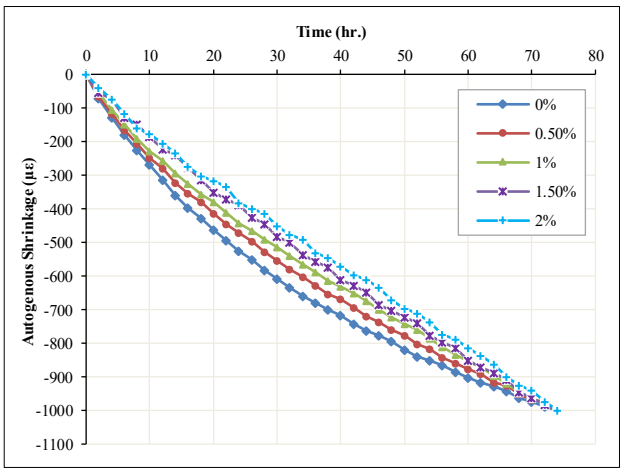

(d) Autogenous shrinkage of specimen after curing at 105°C

Figure 8. Early age of drying and autogenous shrinkage of specimens after curing at 60 °C and 105 °C

In contrast, alkali-activated pastes tend to show significantly higher autogenous shrinkage. While, the autogenous shrinkage of low calcium fly ash for precast application was found to be ranging between 550 με and 750 με [52]. The autogenous shrinkage for the cement paste with water to cement ratio of 0.40 is reported previously and the value is typically 130 με [53]. For slag in the binder composition, autogenous shrinkage is reported typically in the range of 1400 με to 3800 με [54, 55]. After 30 h., shrinkage progression began to slow down. The results showed that the autogenous shrinkage of porcelain-based geopolymer mortars fell in a broad range from 150 με to 1030 με, depending on the level of PP fiber content and initial curing temperature. The autogenous shrinakges of specimen mortars were 2 to 5 times that of drying shrinkage. Similar results were reported by others with slag [56] and fly ash type F [57]. Additional, the development of autogenous shrinkage of porcelain based geopolymer mortars behaved analogously, as it increased rapidly in the first 7 days followed a gradual growth up to 14 days. This characteristic indicates that autogenous shrinkage of porcelain based geopolymer mortars primarily occurs at the early stage of alkali activation. Furthermore, specimens cured at a high initial temperature of 105°C exhibit the most pronounced early-age drying shrinkage when compared to those specimens cured at 60 °C, particularly within the first 30 h. However, temperature had a lesser significant influence on autogenous shrinkage, which began to decline after the 33rd h. These trends are consistent with prior studies by Bakharev et al. [58] and Ye & Radlinska [59], which reported that curing at 60°C-80°C reduces drying shrinkage.

Figures 9-a to 9-d illustrated the drying and autogenous shrinkage behavior of specimens cured at 60 °C and 105 °C, measured at various ages of 3, 7, 14, 21, 28, 60, 90, and 120 days. These figures provide a comparative analysis of shrinkage progression over time, highlighting the influence of curing temperature on both early-age and long-term shrinkage characteristics. In line with early-age shrinkage trends, specimens cured at 105 °C exhibited a significantly higher shrinkage value compared to those specimens cured at 60 °C. Compares the 14-day period, the shrinkage rate gradually declined with time. Increasing the PP fiber content resulted in shrinkage reduction, indicating the effectiveness of fiber reinforcement in restraining volumetric deformations of geopolymer mortar. As evident in Figures 9-a and Figure 9-b. Despite this incident, specimens exposed to elevated initial curing temperatures continued to show higher shrinkage rates than those specimens cured at 60 °C. Interestingly, when the curing temperature exceeded 90 °C, the effectiveness of fiber reinforcement became more pronounced, particularly from day 14 onward (Figure 9-c and 9-d).

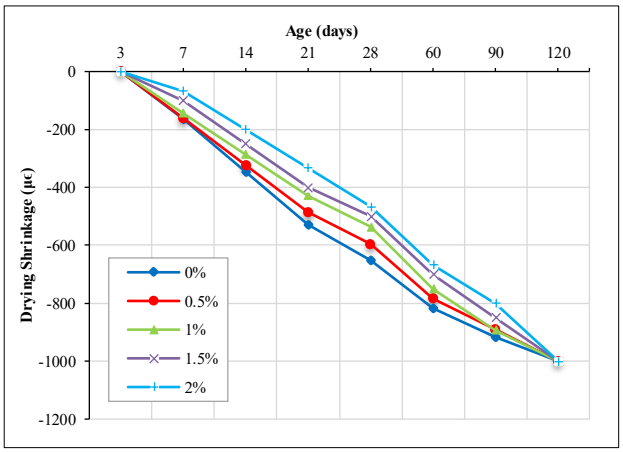

(a) Drying shrinkage of specimen after curing at 60°C

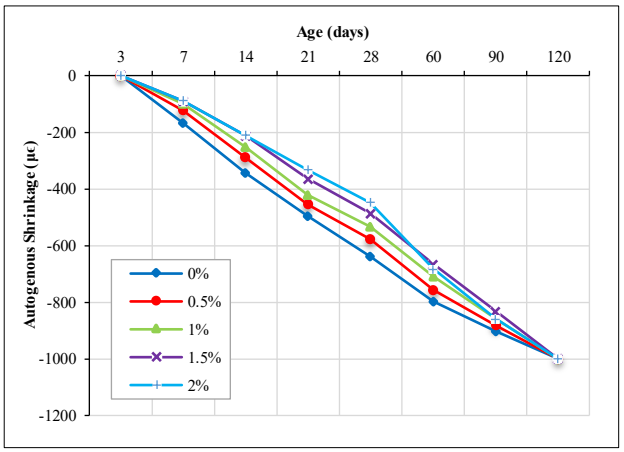

(b) Autogenous shrinkage of specimen after curing at 75°C

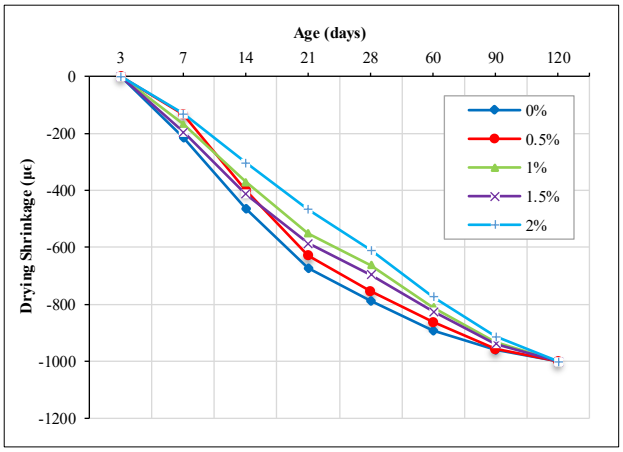

(c) Drying shrinkage of specimen after curing at 90 °C

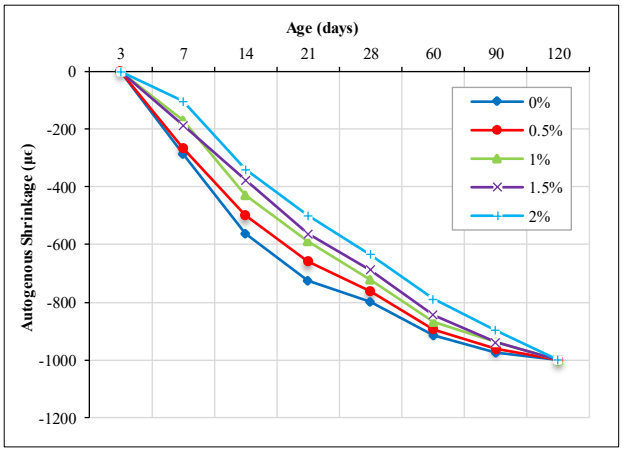

(d) Drying shrinkage of specimen after curing at 105 °C

Figure 9. Long term shrinkages of specimens after curing at 60 °C and 105 °C

At 120 days, the drying shrinkage values of specimens cured with 105°C with varying PP fiber contents (0%, 0.5%, 1.0%, 1.5%, and 2.0%) were recorded as 1814με, 1361με, 1088 με, 816με, and 544με respectively (Table 5). In contrast, specimen containing 0% PP fiber and cured at 60°C exhibited the lowest drying shrinkage value of 114με. The highest autogenous shrinkage was observed in the specimen with 0% PP fiber cured at 105°C, measuring 485με. The results clearly demonstrate that drying shrinkage decreases as the PP fiber content increases. This trend aligns with findings from previous studies, such as those by Wongsa et al. [60], which reported similar shrinkage reduction in geopolymer mortars containing PP fiber. The presence of PP fiber, particularly in low calcium porcelain matrices, refined the pore structure by reducing capillary pore size and enhancing the overall pore network. These microstructural changes were confirmed through scanning electron microscopy (SEM) analysis conducted in this study. Overall, the incorporation of PP fiber proved effective in mitigating drying shrinkage in porcelain-based geopolymer mortars.

Table 5. Shrinkage of specimens under various curing temperatures

PP (%)	Average rate of shrinkage															
	(24 h)								(72 h)							
	Drying (με)				Autogenous (με)				Drying (με)				Autogenous (με)			
	Curing temperature (°C)								Curing temperature (°C)							
	60	75	90	105	60	75	90	105	60	75	90	105	60	75	90	105
0	489	537	570	611	388	459	483	524	2250	2380	2610	3580	670	740	890	1030
0.5	462	500	543	560	346	407	448	469	1190	1320	1730	3120	490	540	580	830
1	425	466	511	512	300	371	406	441	800	1030	1330	2710	300	350	590	680
1.5	392	421	481	480	285	344	354	388	560	830	1080	2290	210	290	310	540
2.0	370	367	439	439	266	333	333	392	270	490	820	1890	150	240	240	280
	60 days								120 days							
	Drying (με)				Autogenous (με)				Drying (με)				Autogenous (με)			
	Curing temperature (°C)								Curing temperature (°C)							
	60	75	90	105	60	75	90	105	60	75	90	105	60	75	90	105
0	816	843	893	932	796	826	882	915	490	890	1042	1814	285	310	340	485
0.5	784	824	862	912	756	796	844	896	370	680	782	1361	242	264	289	412
1	750	782	810	879	709	770	812	867	280	550	625	1088	199	217	234	338
1.5	700	732	825	846	667	737	789	844	200	373	469	816	156	171	180	263
2.0	667	704	773	809	684	694	772	789	150	270	313	544	114	124	136	194

Table 6 presented the percentage reduction in shrinkage across different fiber contents. During the 4-day interval from day 3 to day 7, shrinkage values were highest. The reduction in drying shrinkage for specimens containing 0%, 0.5%, 1.0%, 1.5%, and 2.0% PP fiber was 42.11με/day, 40.54με/day, 35.71με/day, 25.00με/day, and 21.93με/day, respectively. Similarly, the reduction in autogenous shrinkage over the same period was 40.82με/day, 30.99με/day, 25.13με/day, 22.44με/day, and 16.67με/day respectively. At a curing temperature of 105 °C, the effectiveness of fiber reinforcement became even more pronounced. The reduction in drying shrinkage for fiber reinforced specimens increased to 71.13με /day, 66.75με/day, 45.96με/day, 47.49με/day, and 35.85με/day respectively. The reduction in autogenous shrinkage was 67.53με/day, 47.76με/day, 42.16με/day, 46.58με/day, and 25.77με/day when fiber addition to specimen increased from 0%, 0.5%, 1.0%, 1.5%, and 2%. These findings confirm that PP fiber significantly mitigates both drying and autogenous shrinkage, particularly under elevated curing temperatures. The higher curing temperature, the more effective the fiber reinforcement appears to be in controlling shrinkage behavior. PP fiber were highly effective during the early ages of curing, especially under high temperature conditions. Their influence became less pronounced over time. This suggests that the shrinkage-controlling benefits of PP fiber is most impactful during the initial hydration and setting phases, when internal stresses and moisture loss are most critical. PP fiber was more effective at reducing drying shrinkage than autogenous shrinkage.

Table 6. Change in shrinkage of specimens

Duration (day)	Reduction in shrinkage (με per day) at 60°C curing temperature									
	Drying					Autogenous				
	Fiber (%)					Fiber (%)				
	0%	0.5%	1.0%	1.5%	2.0%	0%	0.5%	1.0%	1.5%	2.0%
3→7	42.11	40.54	35.71	25.00	21.93	40.82	30.99	25.13	22.44	16.67
7 → 14	26.24	23.61	21.54	21.43	19.05	25.06	23.17	20.41	17.40	17.54
14 → 21	26.24	23.61	24.41	21.98	19.05	21.55	23.17	20.41	21.43	17.54
21→ 28	17.49	17.71	15.79	17.40	19.05	20.55	15.44	15.31	14.29	16.29
28 → 60	5.10	5.91	6.70	6.25	7.40	4.93	5.55	5.50	5.61	6.25
60 → 90	3.51	4.27	5.03	5.56	5.85	3.40	3.60	4.76	5.00	4.44
90 → 120	3.27	3.86	4.69	5.56	6.67	2.72	3.60	3.57	5.00	4.68
Duration (day)	Reduction in shrinkage (με per day) at 105°C curing temperature									
	Drying					Autogenous				
	Fiber (%)					Fiber (%)				
	0%	0.5%	1.0%	1.5%	2.0%	0%	0.5%	1.0%	1.5%	2.0%
3→7	71.13	66.75	45.96	47.49	35.85	67.53	47.76	42.16	46.58	25.77
7 → 14	40.16	40.94	37.19	32.04	33.87	39.76	33.29	32.83	27.16	29.41
14 → 21	29.53	29.39	29.81	24.51	26.26	23.27	22.54	22.82	26.62	22.83
21→ 28	10.31	15.74	19.02	17.93	19.15	2.99	14.91	16.15	14.88	15.76
28 → 60	3.67	4.17	4.53	4.87	5.17	2.58	3.70	4.48	4.86	4.83
60 → 90	1.92	2.18	2.57	3.17	3.61	1.47	2.06	2.37	2.86	3.19
90 → 120	0.89	1.29	2.07	2.29	3.44	0.81	0.88	1.47	2.03	3.19

Note: (-) decreased

Initial curing temperature also played a critical role in early-age shrinkage behavior. Shrinkage magnitude declined progressively with age, with minimal changes recorded between 90 and 120 days. For specimens cured at 60 °C, the change in drying shrinkage for PP fiber contents of 0%, 0.5%, 1.0%, 1.5%, and 2.0% was 3.27%, 3.86%, 4.69%, 5.56%, and 6.67% respectively. Under 105 °C curing conditions, the corresponding changes were 0.81%, 0.88%, 1.47%, 2.03%, and 3.19%. In comparison, the reduction in autogenous shrinkage at 60 °C was 3.27%, 3.86%, 4.69%, 5.56%, and 6.67%, while at 105 °C it was 0.89%, 1.29%, 2.07%, 2.29%, and 3.44% respectively. These findings suggest that the primary driving forces behind shrinkage are capillary stress and disjoining pressure, which contribute to time-delayed viscoelastic and viscoplastic deformations, as discussed by Rudic et al. [60] and Ye & Radlinska [61]. Notably, the highest drying shrinkage in porcelain-based geopolymer mortar was observed that revealed a linear relationship between fiber content and shrinkage reduction. To further explore this behavior, the authors compared results with the findings of Ye et al. [62] which provided understanding the interplay between microstructural evolution and shrinkage mechanisms in geopolymer systems.

4.3.2. The Effect of High Alkali Concentration

Regarding the effect of high alkali concentration, the 90-day drying shrinkage rates revealed a direct correlation between increased alkali concentration and elevated shrinkage levels. Specifically, mortars activated with a 14M alkali solution exhibited significantly higher drying shrinkage compared to those specimens with lower concentrations. This increase in shrinkage is attributed to the formation of a finer pore structure, which induces higher capillary stresses during moisture loss [63]. Elevated activator concentrations enhance the dissolution and depolymerization of aluminosilicate phases in porcelain, promoting the incorporation of alkali metal cations into the geopolymer matrix. This process strengthens the binding of alkali ions within the structure while reducing the presence of excess free alkali cations and other mobile ions in the system [64]. Specimens subjected to higher initial curing temperatures exhibited increased shrinkage. This behavior is likely due to accelerated reaction kinetics and rapid moisture loss at elevated temperatures, which intensify capillary stresses and promote microstructural densification, ultimately leading to greater shrinkage [65].

4.4. Fresh Properties of Porcelain-Based Geopolymer Concrete

4.4.1. Slump

The fresh properties of porcelain-based geopolymer concrete with varying PP fiber contents were presented in Table 7. The correlations between slump against compaction factor, and between slump against Vebe time were illustrated in Figure 10-a and Figure 10-b respectively. The results from slump, compaction factor and Vebe time tests show consistent trends, indicating that increasing PP fiber content reduces workability across all measured parameters. When activated with 14M sodium hydroxide and reinforced with 0%, 0.5%, 1.0%, 1.5%, and 2.0% PP fiber, the slump values were 257 mm, 142 mm, 63 mm, 44 mm, and 7 mm respectively. PP fiber addition caused significant slump reductions of 44.74%, 75.52%, 82.87%, and 97.27% as fiber content increased. The steepest drop occurred at 0.5% and 1.0% fiber content (44.74%→75.52%), with further decreases at 1.5% and 2.0% (82.87%→97.27%). This loss of workability is linked to the high molarity of the alkaline activator and the fibers' tendency to increase internal friction and particle interlocking. These results align with findings by Parthiban et al. [66] and Saloni et al. [67] reported similar effect of fiber incorporation on slump behavior. For rheology and fresh stability, fiber entanglement and increased particle friction elevate yield stress and viscosity, reducing slump and affecting entrapped air and consolidation, which in turn influence hardened-state porosity and strength. To maintain workability at high fiber volumes, increasing superplasticizer dosage is recommended. Compared with low-calcium binder like slag, porcelain particles have lower angularity and a more spherical shape, improving flowability and reducing shear resistance [68]. This morphology resulted from a two-stage size reduction. Primary crushing process followed by fine grinding process which produced rounder and more uniform particles. Under similar conditions, porcelain-based geopolymer concrete showed better flow than slag-based systems. Zuaiter et al. [69] reported a maximum slump of 160 mm. for slag–fly ash mixes, 37.74% lower than that of porcelain-based mixes.

Table 7. Workability of porcelain based geopolymer concrete

Fiber content (%)	Slump (mm)	Change in Slump (%)*	Compaction Factor	Change in Compaction Factor (%)*	Vebe Time (sec)	Change in Vebe Time (%)*
0	257	-	0.97	-	4.26	-
0.5	142	-44.74	0.90	-7.22	5.20	18.07
1.0	63	-75.52	0.80	-17.53	6.81	37.44
1.5	44	-82.87	0.76	-21.64	7.40	42.43
2.0	7	-97.27	0.71	-26.80	9.20	53.69

* With respect to the porcelain based geopolymer concrete without PP fiber

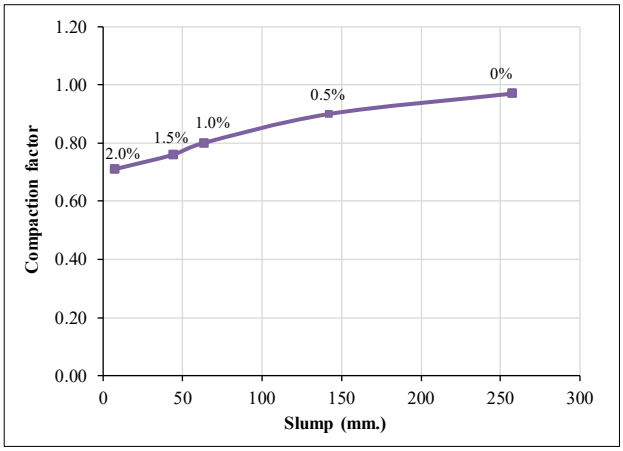

(a) Relationship between compaction factor against slump

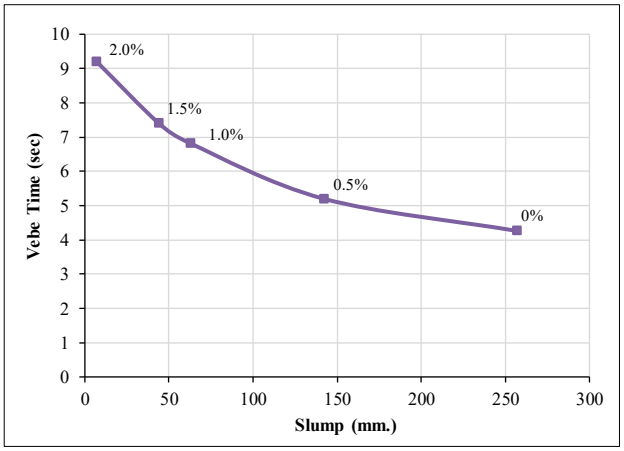

(b) Relationship between Vebe Time and slump

Figure 10. Correlation between compaction factor, Vebe time and slump for geopolynmer concrete mixes

4.4.2. Compaction Factor

Figure 10-a illustrated the relationship between compaction factor and slump, indicating that lower PP fiber content corresponds to higher slump values. The compaction factor results closely matched the trends observed in the slump test. The control mix without PP fiber recorded the highest compaction factor of 0.97. The inclusion of PP fiber at 0.5%, 1.0%, 1.5%, and 2.0% by volume reduced the compaction factor by 7.22%, 17.53%, 21.64%, and 26.80%, respectively. The most significant reduction in compactability occurred between 0.5% and 1.0% fiber content (7.22% → 17.53%), while further increases to 1.5% and 2.0% fiber content resulted in a more gradual decline (21.64% → 26.80%). This reduction is attributed to the increased likelihood of fiber interlocking at higher PP fiber dosages [62]. PP fiber possess high tensile strength and elastic modulus, and their hydrophobic nature contributes to weak bonding with the

cementitious matrix. The critical fiber content range of 0.5–1.0% represents a percolation threshold, beyond which previously dispersed fibers begin to interconnect and form a continuous network within the geopolymer matrix. This network disproportionately increases the matrix's resistance to deformation, leading to a pronounced rise in yield stress and a rapid decline in workability. At lower fiber dosage (0.5%), the binder matrix remains sufficiently continuous to coat and lubricate individual fibers, thereby sustaining acceptable flow characteristics. However, once the percolation threshold is surpassed, the surface area requiring wetting and lubrication expands more rapidly than the available paste volume can accommodate. This imbalance results in localized stiffening, entrapped voids, and an abrupt deterioration in compactability.

4.4.3. Vebe Time

Table 7 presented the Vebe time measurements for porcelain-based geopolymer concrete. The addition of PP fiber at 0.5% and 1.0% by volume caused modest increases in Vebe time of approximately 18.07% and 37.44% respectively. At the highest dosage of 2.0% fiber content, Vebe time rose by 53.69%, indicating a substantial reduction in workability at elevated fiber contents. Above 1.0% fiber content, the increase in Vebe time became more pronounced. Mixes incorporating 1.5% and 2.0% PP fiber exhibited significantly extended Vebe times compared to those containing 0.5% and 1.0% fiber content, indicating a notable reduction in workability with higher fiber dosage. This trend reflects the negative impact of higher fiber volumes on workability. It was primarily due to increased internal friction and reduced flowability. For mixes activated with 14M sodium hydroxide, the recorded Vebe times for 0%, 0.5%, 1.0%, 1.5%, and 2.0% PP fiber content were 4.26, 5.20, 6.81, 7.45, and 9.22 seconds respectively. These results confirm that increasing fiber content impairs the fresh workability of geopolymer concrete, consistent with the patterns observed in slump flow and flow table test of mortars. Figure 10-b illustrated the inverse relationship between Vebe time and slump, showing that Vebe time decreases markedly as fiber content is reduced.

4.4.4. Segregation and Bleeding

The liquid content in porcelain-based geopolymer paste plays a crucial role in shaping its workability. It was found that the surface of specimens remained moist after placing into molds. Mixtures containing larger volumes of PP fiber showed less bleeding compared with mixtures containing fewer fibers content. Similar result was found by Posi et al. [70]. He reported that none of the mixtures exhibited bleeding or segregation during mixing, placement, or compaction. This suggests that PP fiber contribute to matrix stability by restricting the movement of free water and improving internal cohesion. PP fiber reduce permeability of specimens by encouraging the formation of gel products and reduce bleeding via briding effect. The PP fiber densify the matrix and limit water migration. The PP fiber form a mesh-like structure in the fresh mix that helps retain water and fine particles, preventing water from rising to the surface. PP fiber also enhance the mix's cohesiveness, particularly under low workability coniditon, ensuring uniform material distrucution and reducing the risk of segregation.

4.5. Absorption and Porosity

4.5.1. Absorption

Figures 11 and 12 illustrated the water absorption behavior of porcelain-based geopolymer concrete specimens reinforced with varying PP fiber contents. At 28 days, the water absorption rates for specimens activated with 14M sodium hydroxide and containing 0.5%, 1.0%, 1.5% and 2.0% PP fiber were recorded as 6.28%, 6.06%, 5.97% and 5.79% respectively. These results indicate that both increasing fiber content and extended curing time contribute to reduced water absorption.

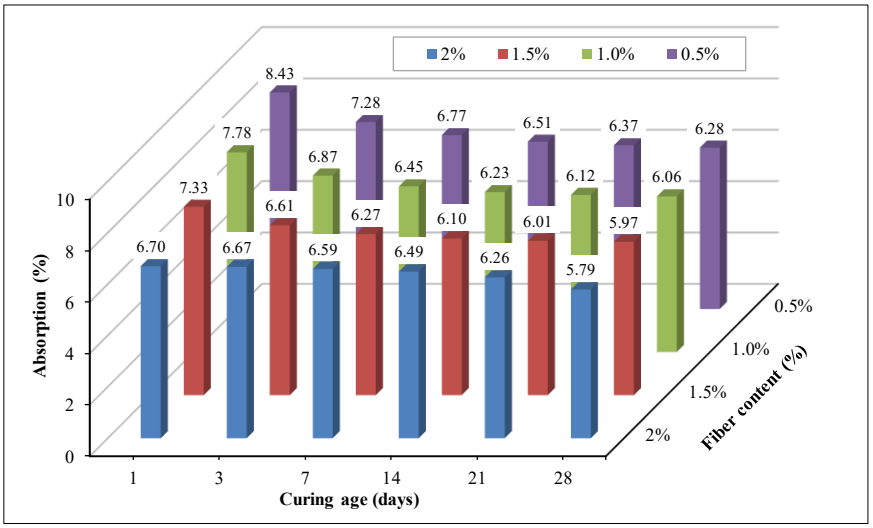

Figure 11. Absorption of porcelain based geopolymer concrete

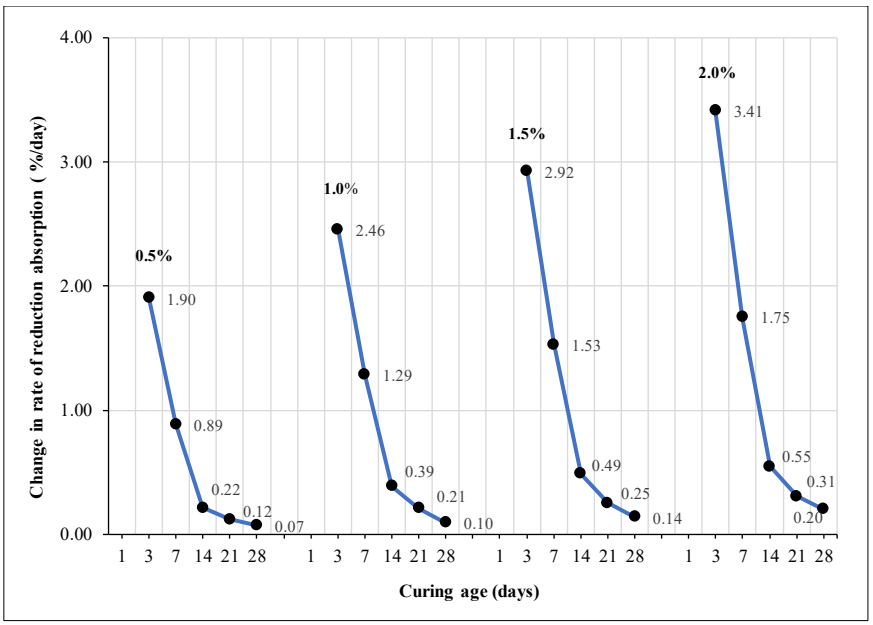

Figure 12. Reduction in absorption rate

Similar trends were observed in specimens cured at 1, 3, 7, 14 and 21 days. Ye et al. [71] identified critical pore size as a key factor influencing permeability, with gel pores playing a dominant role in water transport. Jennings [72] further emphasized the impact of pore structure on drying and autogenous shrinkage. In this study, the highest water absorption rate (8.43%) was recorded with the 1-day specimen mixed with 0.5% PP fiber. It was noticed that large pores were still present.

Between 21 and 28 days of curing, water absorption of specimmens decreased gradually, with daily reduction rates of 0.07%, 0.10%, 0.14% and 0.20% for mixes containing 0.5%, 1.0%, 1.5%, and 2.0% PP fiber respectively. In early-age specimens (3 days), the reduction in porosity was more pronounced. Water absorption rates declined by 1.90%, 2.46%, 2.92% and 3.41% per day across the same fiber dosages. The most significant decrease in water absorption occurred within the first three days, particularly in the mix with 2.0% fiber content. These findings indicate that porcelain-based geopolymer concrete becomes increasingly impermeable over time as pores are progressively filled by geopolymerization products. The incorporation of PP fiber enhances this effect, especially at early ages. High curing temperatures are essential to accelerate the geopolymerization process when early-age strength and durability are required. Porosity results test further confirms that specimens with PP fiber exhibit lower total porosity due to a reduction in interconnected pores within the matrix, contributing to improved durability and reduced permeability.

4.5.2. Porosity

Figures 13 and 14 illustrated the influence of PP fiber content on the porosity of porcelain-based geopolymer concrete. The results show that porosity decreases with both increasing PP fiber content and extended curing time. However, the rate of porosity reduction diminished as curing progressed. The most significant changes in porosity values occurred at early ages. At 28 days of curing, the porosity values of specimens containing 0.5%, 1.0%, 1.5%, and 2.0% PP fiber are recorded as 10.61%, 12.07%, 12.80%, and 13.42% respectively. The corresponding daily reduction rates in porosity are 0.19%, 0.25%, 0.29%, and 0.33%, respectively. These findings indicate that while porosity continues to decline over time, the reduction rate slows as the matrix matures. This trend mirrors the behavior observed in water absorption tests, where early-age specimens exhibited more pronounced reductions. The porosity values declined rapidly during the first-seven days, indicating active geopolymerization and consequent pore refinement, particularly in fiber-reinforced mixes. Overall, the incorporation of PP fiber contributes to a denser microstructure and improved durability by reducing interconnected pore networks. PP fibers act as physical barriers that interrupt capillary continuity and promote microstructural densification by aiding the retention of reaction products within pore spaces; higher fiber volumes enhance early pore blocking and local densification.

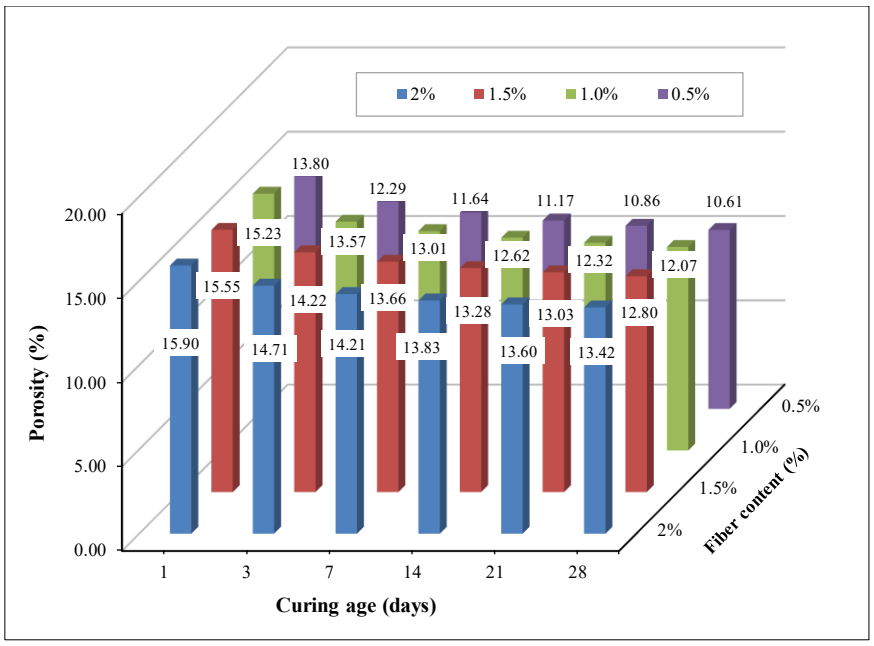

Figure 13. Porosity of porcelain based geopolymer concrete

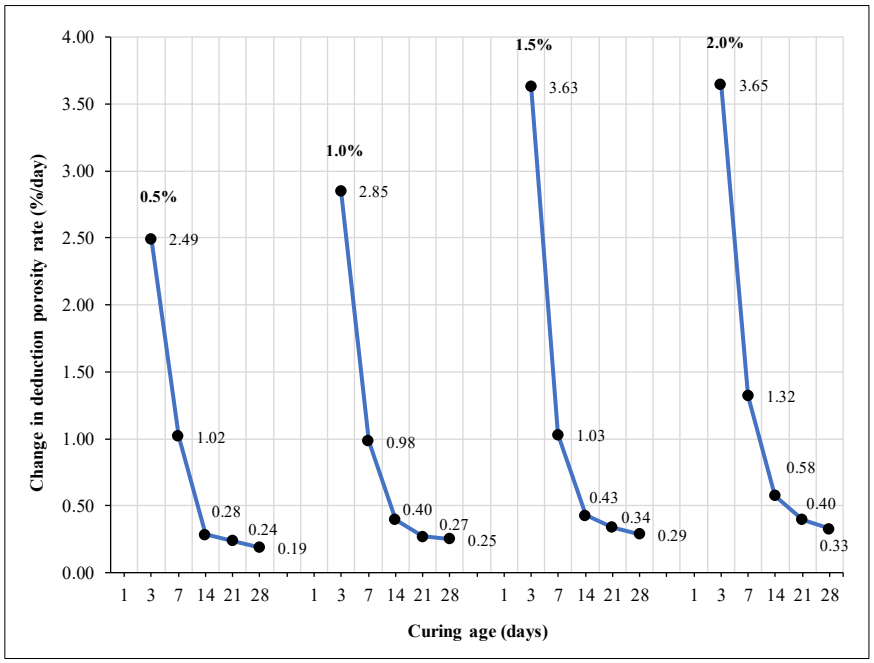

Figure 14. Reduction in porosity rate

4.6. Compressive Strength and Splitting Tensile Strength

4.6.1. Compressive and Splitting Tensile Strength

Figure 15. presented the compressive strength results of porcelain-based geopolymer concrete reinforced with varying PP fiber contents, measured at curing ages of 1, 3, 7, 14, 21, and 28 days. The results show a consistent increase in compressive strength with both longer curing durations and higher fiber content. The lowest compressive strength was observed in the 1-day specimen containing 0.5% PP fiber, while the highest strength was recorded at 28 days in the mix with 2.0% PP fiber. At 3 days of curing, the compressive strengths for mixes with 0.5%, 1.0%, 1.5% and 2.0% PP fiber were 27.55 N/mm², 30.33 N/mm², 32.98 N/mm², and 36.22 N/mm² respectively. These results confirm that increasing fiber content enhances early-age strength. Incremental increases in fiber dosage from 0.5% to 1.0%, 1.0% to 1.5%, and 1.5% to 2.0% resulted in compressive strength gains of 10.09%, 8.74%, and 10.20% respectively. The continuous improvement in strength with curing time suggests active geopolymerization and matrix densification.

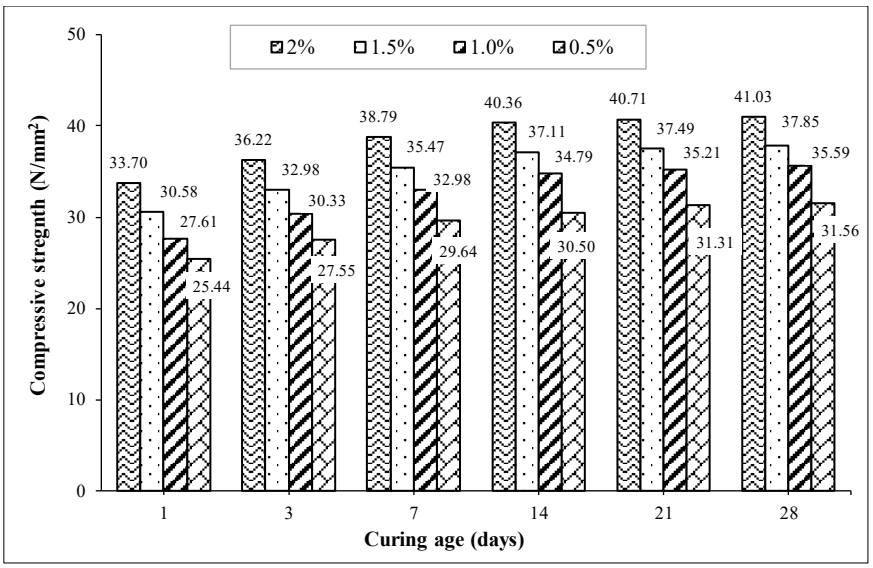

Figure 15. Compressive strength mixed with different PP contents

The enhanced compressive strength is attributed to the role of PP fiber as microstructural bridges that reinforce the matrix, reduce crack propagation and promote a more homogeneous and compact internal structure. This bridging effect contributes to the overall integrity and durability of the geopolymer concrete. At 14 days, the compressive strength of porcelain-based geopolymer specimens increased with both higher PP fiber volume fractions and extended curing time. By 28 days, the compressive strengths of specimens containing 0.5%, 1.0%, 1.5%, and 2.0% PP fiber were recorded as 31.56 N/mm², 35.59 N/mm², 37.85 N/mm², and 41.03 N/mm² respectively. The addition of 0.5% fiber resulted in strength increases of 12.77%, 6.35%, and 8.40% when compared to the preceding fiber levels.

However, the percentage increase in compressive strength at 28 days was lower than those observed at earlier curing ages (7 and 14 days), which is consistent with the typical strength development pattern of ordinary Portland cement systems. This suggests that the majority of strength gain in geopolymer concrete occurs during the early curing period. Furthermore, specimens subjected to an initial curing temperature of 105 °C for 24h. Exhibited significantly enhanced early-age strength at 1, 3, and 7 days. The rate of compressive strength development per day, as shown in Table 8, peaked during the first-three days of curing and then declined sharply as the matrix matured toward 28 days. This rapid early strength gains highlights the importance of thermal curing in accelerating geopolymerization and improving early mechanical performance. Rapid early geopolymerization converted reactive aluminosilicate phases into binding gels that fill capillary and gel pores, producing a rapid drop in measured porosity values. In the mid age (14 days- 21 days), gel continued to densify and reorganize at a slower rate, producing diminishing daily reductions in porosity and slower strength gained as the system approached a more stable microstructure. Available reactive silica and alumina, alkali concentration, and soluble silicon determine the pace and extent of gel growth. However, insufficient activator or imbalanced SiO_2/Al_2O_3 limits network formation and leaves residual capillary porosity. The quality of interfacial transition zone (ITZ) forms around aggregates and fiber depends on local reaction product accumulation, pore-filling, and mechanical interlock, and strongly influences splitting tensile behavior.

Table 8. Change in compressive strength

PP (%)	Change in compressive strength (N/mm²/day)					Change in splitting tensile strength (N/mm²/day)				
	1→3	3→7	7→14	14→21	21→28	1→3	3→7	7→14	14→21	21→28
0.5	2.50	1.89	0.41	0.38	0.11	3.54	3.10	0.66	0.56	0.32
1.0	2.46	2.18	0.78	0.17	0.15	3.22	3.05	1.25	0.46	0.45
1.5	1.96	1.88	0.66	0.14	0.14	2.95	2.47	1.01	0.36	0.31
2.0	1.87	1.77	0.58	0.12	0.11	2.63	1.98	1.09	0.35	0.29

Similar trends were observed in the splitting tensile strength results, as shown in Figure 16. The influence of PP fiber content on splitting tensile strength was more pronounced than its effect on compressive strength. At 28 days of curing, the splitting tensile strengths of 14M-activated porcelain-based geopolymer concrete mixes containing 0.5%, 1.0%, 1.5%, and 2.0% PP fiber were 6.30 N/mm², 6.60 N/mm², 7.12 N/mm², and 7.65 N/mm², respectively. Compared to the 1-day cured specimens, the 28-day mixes showed strength improvements of 62.37%, 46.67%, 37.71%, and 35.79% for the respective fiber contents. The rate of strength gain per day in splitting tensile strength was higher than that observed in compressive strength tests, indicating more rapid development of tensile capacity in fiber-reinforced mixes.

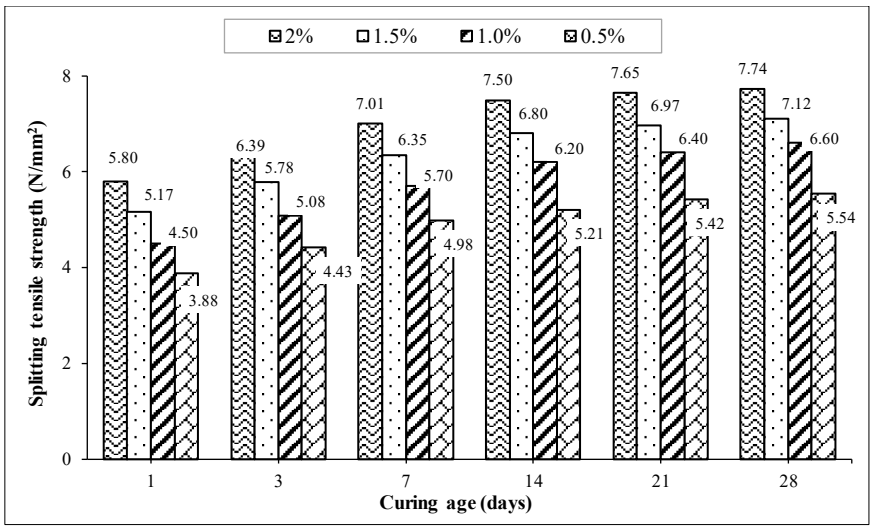

Figure 16. Splitting tensile strength mixed with different PP Contents

The enhancement in splitting tensile strength is attributed to the increased formation of calcium silicate hydrate (C–S–H) gel and the reinforcing effect of PP fibers, which densify the internal matrix structure. The PP fiber act as micro-bridges, improving crack resistance and load distribution, thereby contributing to the overall tensile performance. These findings are consistent with studies by Palmer et al. [73] which also reported early-age strength improvements in fiber-reinforced geopolymer systems. Additionally, the SiO_2/Al_2O_3 molar ratio plays a positive role in promoting geopolymerization and enhancing mechanical properties. Importantly, no adverse effects such as fiber aggregation or pore formation were observed at fiber contents up to 2%, confirming the compatibility of PP fiber with the porcelain-based geopolymer matrix. Similar conclusions were drawn by Rajak & Rai [74] in their respective studies.

4.6.2. The Correlation between Compressive and Splitting Tensile Strength

The results confirmed that increasing PP fiber content in porcelain-based geopolymer concrete led to enhanced splitting tensile strength. At early curing ages, the ratio of splitting tensile strength to compressive strength ranged from 0.155 to 0.172. By 28 days, the ratio increased between 0.176 and 0.189, indicating a progressive improvement in tensile performance relative to compressive strength over time. These trends are consistent with findings in both conventional concrete and geopolymer concrete reinforced with natural fibers [75] and synthetic fibers [76]. Figure 17 presented the detailed ratios of splitting tensile to compressive strength for each mix. Figure 18 illustrated the relationship between porosity and mechanical strength. At early ages (3 to 7 days), splitting tensile strength increased rapidly, while matrix porosity decreased sharply. As curing progressed, the rate of porosity reduction declined, but the inverse relationship between porosity and strength remained evident. This trend was also found in 28-day cured specimens, as reported by Chen et al. [77]. However, porosity was found to inversely correlate with both compressive and splitting tensile strength, confirming that a denser microstructure contributes to improved mechanical performance. Additionally, reduced water absorption at 28 days was associated with higher strength values, further supporting the role of pore refinement in durability enhancement. Similar observations were made by Farhana et al. [78] reinforcing the link between reduced permeability and improved strength in geopolymer systems.

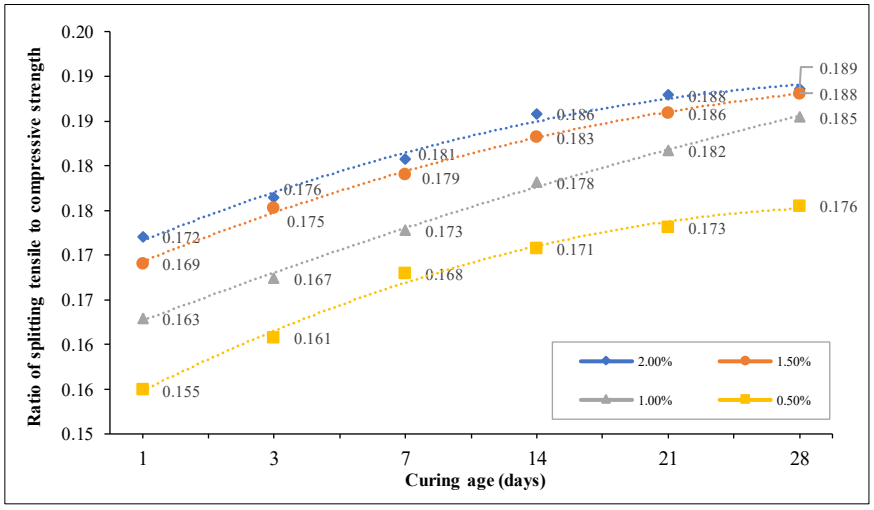

Figure 17. Ratio splitting tensile strength to compressive strength with different PP contents

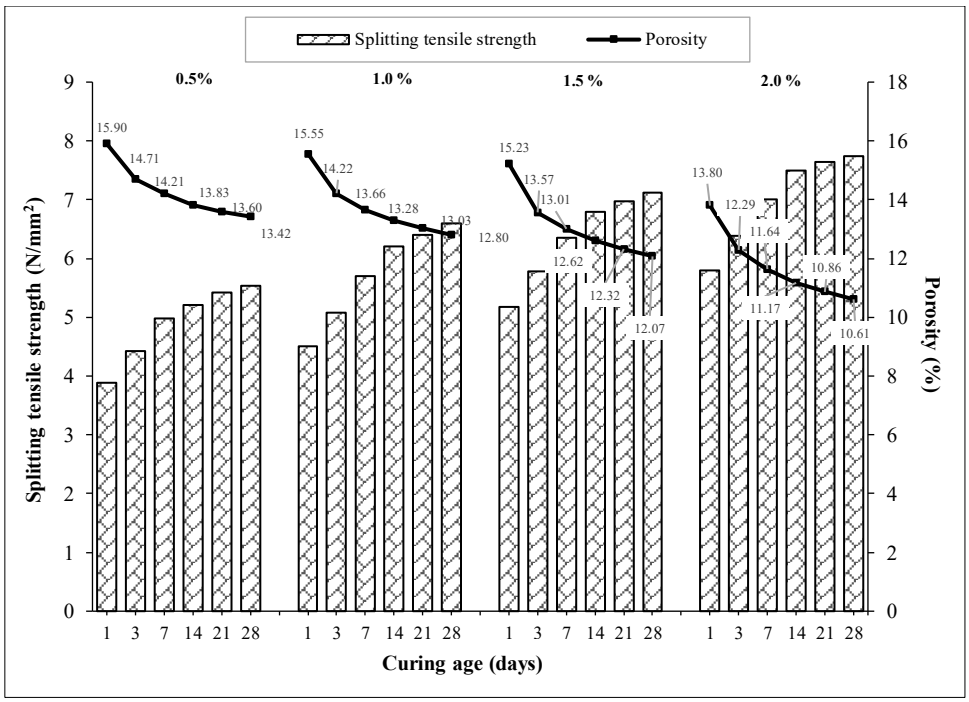

Figure 18. Relationship between splitting tensile strength and porosity

Figure 19 presented a comparison between the experimentally obtained splitting tensile strength and predicted values derived from previous studies. At early age (7 days), the experimental specimens exhibited higher splitting tensile strength than the reference materials. The splitting tensile strength increased with both PP fiber content and the curing duration. As shown in Figure 20, the splitting tensile strength of the tested specimens at 28 days was higher than that of conventional materials, including normal concrete, high-strength and normal-weight concrete, as well as geopolymer concretes incorporating fly ash Type F and Type C. The predictive formulas used for estimating splitting tensile strength were based on specimens without fiber reinforcement. Consequently, the observed tensile strength values exceeded those predicted by these models. The percentage differences between the predicted and experimental results were presented in Table 9. These findings highlight the beneficial effect of PP fiber reinforcement in enhancing the mechanical performance of porcelain-based geopolymer concrete.

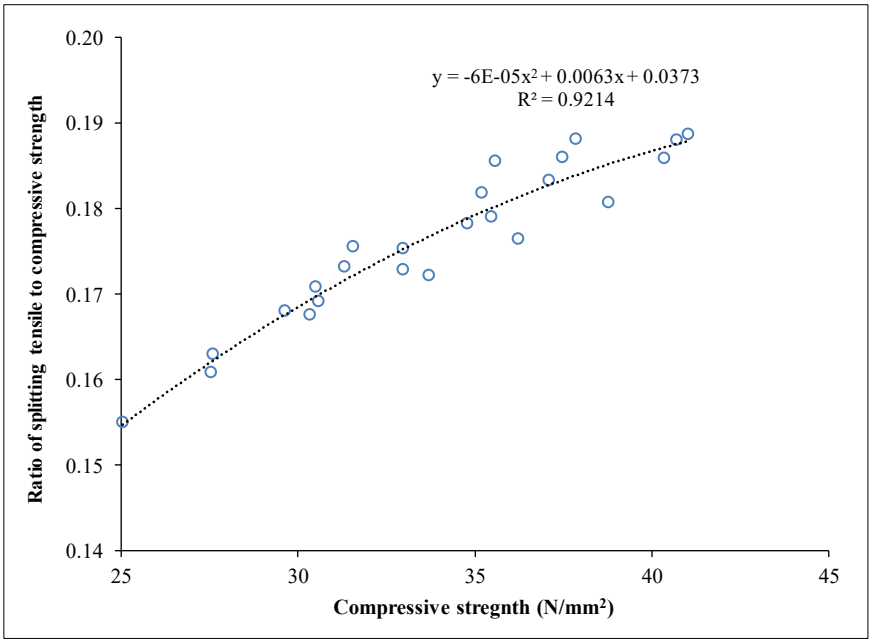

Figure 19. Relationship between ratio splitting tensile to compressive strength at 7 days

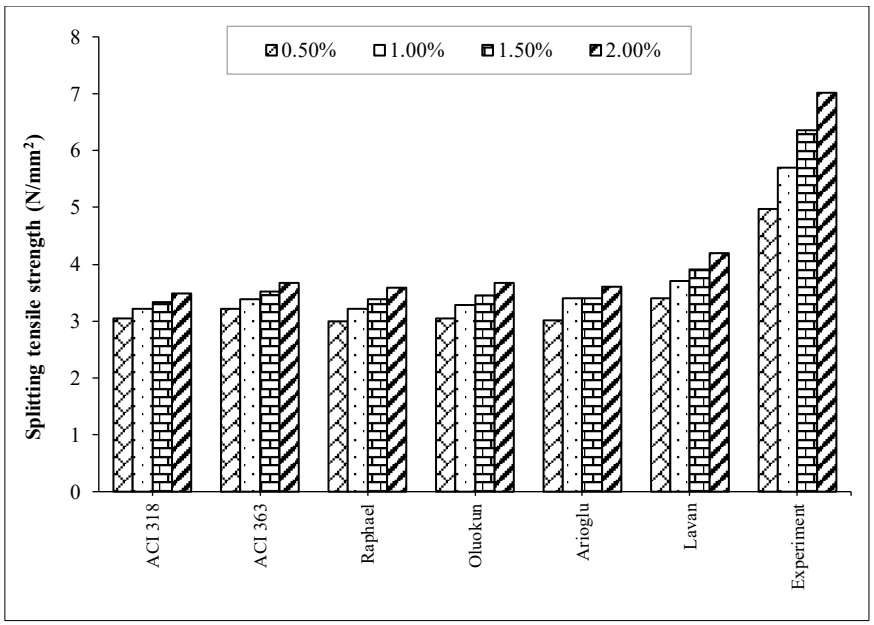

Figure 20. Comparative splitting tensile strength results with others

Table 9. Comparative between predicted and experiment values in splitting tensile strength

PP fiber (%)	Predicted splitting tensile strength by using others proposed formula (N/mm²)					Difference in percentage of strengths compared with others (%)				
	ACI 318 [79]	ACI 363 [80]	Raphael [81]	Lavanya & Jegan [82]	Arıoglu et al. [83]	Difference in tensile (%) $= \left(\frac{f_{cr\,(result)} - f_{cr\,(proposed\ by\ other)}}{f_{cr\,(proposed\ bu\ others)}}\right) \times 100$ where $x = \frac{f_{cr}}{\sqrt{f_c}}$				
	Normal concrete	High strength	Normal weight	Geopolymer fly ash type F	Geopolymer fly ash type C					
	$f_{cr} = 0.56\sqrt{f_c}$	$f_{cr} = 0.59\sqrt{f_c}$	$f_{cr} = 0.313f_c^{0.667}$	$f_{cr} = 0.294f_c^{0.69}$	$f_{cr} = 0.249f_c^{0.772}$	ACI 318	ACI 363	Raphael	Lavanya & Jegan [82]	Arıoglu et al. [83]
	28 days	28 days	28 days	28 days	28 days	28 days	28 days	28 days	28 days	28 days
0.5	3.145	3.314	3.129	3.577	3.143	76.00	67.14	77.02	54.87	76.22
1.0	3.340	3.519	3.390	3.924	3.544	97.55	87.51	94.65	68.15	86.18
1.5	3.445	3.629	3.532	4.115	3.544	106.66	96.15	101.54	72.98	100.85
2.0	3.587	3.779	3.728	4.380	3.739	115.77	104.80	107.61	76.69	107.00

4.6.3. Crack Patterns and Failure of Specimens Under Compressive and Tension

Cracks and surface spalling were noticed in porcelain-based geopolymer concrete specimens when subjected to compressive loads at 25 N/mm² (Table 10). As the stress surpassed 30 N/mm², crack growth became more pronounced. These fractures were mainly vertical and diagonal, forming a mix of slanted and upright lines extending along the specimen's height. Secondary cracks began branching out from the original fracture paths, with surface spalling advancing as the load increased. The level of deterioration was influenced by both fiber content and curing time. Specimens mixed with PP fiber demonstrated reduced cracking and less surface damage, implying enhanced structural resilience under compression. Similarly, specimens exposed to longer curing durations showed greater resistance to cracking, underscoring the benefits of fiber inclusion and extended curing in reinforcing the material. At lower PP fiber contents (0.5% and 1.0%), crack length increased rapidly, whereas the rate of crack propagation gradually slowed as fiber content increased. Once the fiber volume reached 2.0%, the reduction in crack growth became only slight. This indicates that higher fiber content enhances the crack-bridging effect of PP fiber in geopolymer specimens. With greater fiber bridging, cracks become more fully developed before failure, allowing the specimen to dissipate more energy during damage. Both the maximum and median crack widths increased with higher fiber content. Moreover, the maximum crack width continued to grow as fiber content rose. This behavior can be attributed to the tendency of fibers to disperse unevenly and form agglomerates at excessive dosages, which reduces their effectiveness in bridging and controlling cracks. The total crack areas decreased with increasing fiber content, further confirming the beneficial role of fiber reinforcement in enhancing the crack resistance of geopolymer composites. However, when fiber content was excessively high, uneven dispersion and fiber agglomeration occurred, which diminished the effectiveness of fiber bridging and reduced its contribution to crack control.

Table 10. Compressive and splitting tensile crack pattern of specimens

Fiber (%)	Cracking due to Compressive Strength Test (day)		Cracking due to Splitting Tensile Test (day)	
	7	28	7	28
0.5				
1				
1.5				
2				

During the splitting tensile test, regardless of their PP fiber content, all specimens exhibited similar failure modes. Failure occurred abruptly once the peak load was reached, characterized by vertically aligned cracks along the specimen's central axis. Crack initiation typically started at the upper end and progressed downward through the cylindrical form. These results are consistent with observations made by Khoso et al. [84] in studies on low-calcium fly ash-based geopolymer concrete, which revealed comparable crack development patterns. In the splitting tensile test, failure patterns were consistent across specimens with varying PP fiber contents. Failure occurred suddenly upon reaching the ultimate load, with cracks forming vertically along the plane of the specimen. Crack initiation typically began at the top and propagated downward through the cylindrical body.

5. Conclusions

The setting time of porcelain-based geopolymer paste increased with higher PP fiber content. This behavior is attributed to the elevated Si/Al ratio in the geopolymer matrix, which slows down the reaction kinetics and extends the setting period. Water absorption of the specimens consistently decreased with longer curing periods. Similarly, increasing the PP fiber content led to a reduction in absorption levels. The lowest water absorption was recorded at 5.79% in specimens cured for 28 days and reinforced with 2.0% PP fiber.

The slump value decreased by up to 97.3% as PP fiber was added to the porcelain-based geopolymer concrete mix. The incorporation of PP fiber at a 0.5% volume led to better workability results, as it reduced the effect of fiber balling and interlocking. An increase in PP fiber content to 2% by volume resulted in a reduction of the compaction factor by 26.8% and an increase in Vebe time by 115.9%, compared with the plain geopolymer concrete mix.

Porosity also declined as PP fiber content increased. The lowest porosity value 10.61% was observed in specimens cured for 28 days with 0.5% PP fiber. These results indicate that both extended curing and fiber reinforcement contribute to a denser and less permeable microstructure in porcelain-based geopolymer concrete. Mechanical and Shrinkage Performance: The incorporation of PP fiber significantly enhanced the compressive strength, splitting tensile strength, and reduced drying shrinkage of the geopolymer paste. These improvements reflect the beneficial role of fibers in reinforcing the matrix and controlling deformation. Microstructural enhancement: PP fiber addition contributed to greater compactness and homogeneity in the porcelain-based geopolymer concrete. This densification of the internal structure led to improved mechanical performance and durability.

The incorporation of PP fiber demonstrated a clear reduction in both drying and autogenous shrinkage rates, with the effect being more pronounced under drying condition. Early-age shrinkage behavior was significantly influenced by the initial curing temperature. The lowest shrinkage values were recorded in specimens containing 2.0% PP fiber cured at 105 °C, with drying and autogenous shrinkage measured at 439 με and 392 με, respectively. In contrast, the highest shrinkage values were observed in specimens without fiber reinforcement (0% PP) cured at 60 °C, exhibiting drying and autogenous shrinkage of 611 με and 524 με, respectively. These findings underscore the effectiveness of PP fiber in mitigating shrinkage, particularly under elevated curing temperatures and during the early stages of geopolymization.

The integration of PP fiber into porcelain-based geopolymer concrete has been shown to improve both compressive and splitting tensile strength. When the fiber content is increased to 2.0%, the material achieves a compressive strength of 41.03 N/mm² and a splitting tensile strength of 7.74 N/mm², indicating a substantial enhancement in mechanical performance.

The crack length and crack area of the specimens both decreased with higher fiber volume fractions. The crack witdth and depth are more exposed with increment of fiber content. These suggests that the incorporation of PP fiber in geopolymer concrete allows cracks to develop more fully, thereby enhancing the specimen's energy dissipation capacity at failure. The growth of these crack parameters is most rapid at lower fiber contents, while the rate of increase gradually slows as fiber content rise. The results indicate that a fiber volume fraction of 2.0% achieves an optimal balance between crack development and energy absorption. However, the addition of a superplasticizer is necessary to maintain the workability of the specimen mixes.

6. Declarations

6.1. Author Contributions

Conceptualization, B.I.N.A.; methodology, B.I.N.A.; validation, B.I.N.A.; formal analysis, B.I.N.A.; investigation, R.K.; resources, B.I.N.A.; data curation, B.I.N.A.; writing—original draft preparation, B.I.N.A.; writing—review and editing, B.I.N.A.; visualization, B.I.N.A.; supervision, B.I.N.A.; project administration, B.I.N.A.; funding acquisition, B.I.N.A. All authors have read and agreed to the published version of the manuscript.

6.2. Data Availability Statement

The data presented in this study are available on request from the corresponding author.

6.3. Funding and Acknowledgments

This work was supported by the research fund of the Rajamangala University of Technology Thanyaburi, authors would like to express our sincere gratitude to the scientific research fund for financial support to the project (Project number: FRB690069/0168).

6.4. Conflicts of Interest

The authors declare no conflict of interest.

7. References

[1] Mejeoumov, G.G., (2007). Improved cement quality and grinding efficiency by means of closed mill circuit modeling. Ph.D. Thesis. Civil Engineering Department, Texas A&M University, TX, United States.

[2] Chen, X., Zhou, M., Shen, W., Zhu, G., & Ge, X. (2018). Mechanical properties and microstructure of metakaolin-based geopolymer compound-modified by polyacrylic emulsion and polypropylene fibers. Construction and Building Materials, 190, 680–690. doi:10.1016/j.conbuildmat.2018.09.116.

[3] Hanumananaik, M., & Subramaniam, K. V. L. (2023). Shrinkage in low-calcium fly ash geopolymers for precast applications: Reaction product content and pore structure under drying conditions. Journal of Building Engineering, 78, 107583. doi:10.1016/j.jobe.2023.107583.

[4] Kucukgoncu, H., & Özbayrak, A. (2024). Microstructural Analysis of Low-Calcium Fly Ash-Based Geopolymer Concrete with Different Ratios of Activator and Binder Under High Temperatures. Arabian Journal for Science and Engineering, 50(11), 8197–8223. doi:10.1007/s13369-024-09266-1.

[5] Celik, A., Yilmaz, K., Canpolat, O., Al-mashhadani, M. M., Aygörmez, Y., & Uysal, M. (2018). High-temperature behavior and mechanical characteristics of boron waste additive metakaolin based geopolymer composites reinforced with synthetic fibers. Construction and Building Materials, 187, 1190–1203. doi:10.1016/j.conbuildmat.2018.08.062.

[6] Assaedi, H., Alomayri, T., Shaikh, F. U. A., & Low, I.-M. (2015). Characterisation of mechanical and thermal properties in flax fabric reinforced geopolymer composites. Journal of Advanced Ceramics, 4(4), 272–281. doi:10.1007/s40145-015-0161-1.

[7] Sun, P., & Wu, H.-C. (2008). Transition from brittle to ductile behavior of fly ash using PVA fibers. Cement and Concrete Composites, 30(1), 29–36. doi:10.1016/j.cemconcomp.2007.05.008.

[8] Ricciotti, L., Roviello, G., Tarallo, O., Borbone, F., Ferone, C., Colangelo, F., Catauro, M., & Cioffi, R. (2013). Synthesis and Characterizations of Melamine-Based Epoxy Resins. International Journal of Molecular Sciences, 14(9), 18200–18214. doi:10.3390/ijms140918200.

[9] Shen, D., Liu, X., Zeng, X., Zhao, X., & Jiang, G. (2020). Effect of polypropylene plastic fibers length on cracking resistance of high performance concrete at early age. Construction and Building Materials, 244, 117874. doi:10.1016/j.conbuildmat.2019.117874.

[10] He, F., Biolzi, L., Carvelli, V., & Feng, X. (2024). A review on the mechanical characteristics of thermally damaged steel and polypropylene hybrid fiber-reinforced concretes. Archives of Civil and Mechanical Engineering, 24(2). doi:10.1007/s43452-024-00880-2.

[11] Boulekbache, B., Hamrat, M., Chemrouk, M., & Amziane, S. (2010). Flowability of fibre-reinforced concrete and its effect on the mechanical properties of the material. Construction and Building Materials, 24(9), 1664–1671. doi:10.1016/j.conbuildmat.2010.02.025.

[12] Zhang, Z.-H., Yao, X., Zhu, H.-J., Hua, S.-D.& Chen, Y., (2009). Preparation and mechanical properties of polypropylene fiber reinforced calcined kaolin-fly ash based geopolymer, Journal of Central South University, 16 (1), 49–52. doi:10.1007/s11771-009-0008-4.

[13] Gholampour, A., Hosseini-Poul, S. M., Nezhad, S. M., Nematzadeh, M., & Ozbakkaloglu, T., (2025). Effect of polypropylene and polyvinyl alcohol fibers on mechanical behavior and durability of geopolymers containing lead slag: Testing, optimization, and life cycle assessment, Construction and Building Materials, 462: 139960. doi:10.1016/j.conbuildmat.2025.139960

[14] Hong, L., Tang, W., Tan, Y., Wang, Y., Guo, B., Gao, P., Zhan, B., & Yu, Q. (2025). Effect of short fibers on non-uniform strain distribution of geopolymer mortar under dry conditions. Construction and Building Materials, 459, 139768. doi:10.1016/j.conbuildmat.2024.139768.

[15] Patil, S.S., & Patil. A.A., (2015) Properties of polypropylene fiber reinforced geopolymer concrete. International Journal of Current Engineering and Technology, 5(4), 2909-2912.

[16] Zhang, H., Sarker, P. K., Wang, Q., He, B., & Jiang, Z. (2024). Comparative fracture properties of ambient-cured geopolymer concrete containing four different fibers in mono and hybrid combinations using digital image correlation. Journal of Building Engineering, 89, 109288. doi:10.1016/j.jobe.2024.109288.

[17] Ríos, J. D., Mínguez, J., Martínez-De La Concha, A., Vicente, M. Á., & Cifuentes, H. (2020). Microstructural analyses of the addition of PP fibres on the fracture properties of high-strength self-compacting concrete by X-ray computed tomography. Construction and Building Materials, 261, 120499. doi:10.1016/j.conbuildmat.2020.120499.

[18] Peng, M. X., Wang, Z. H., Shen, S. H., & Xiao, Q. G. (2014). Synthesis, characterization and mechanisms of one-part geopolymeric cement by calcining low-quality kaolin with alkali. Materials and Structures, 48(3), 699–708. doi:10.1617/s11527-014-0350-3.

[19] Hanumananaik, M., Reddy, M. S. K., & Subramaniam, K. V. (2022). High-temperature performance of low-calcium fly ash–based geopolymers. Journal of Materials in Civil Engineering, 34(5), 04022040. doi:10.1061/(ASCE)MT.1943-5533.0004181.

[20] Huang, D., Liu, Z., Lin, C., Lu, Y., & Li, S. (2024). Effects and mechanisms of component ratio and cross-scale fibers on drying shrinkage of geopolymer mortar. Construction and Building Materials, 411, 134299. doi:10.1016/j.conbuildmat.2023.134299.

[21] Chen, K. Y., Wang, Y. Q., Min, W. L., Chen, J. J., Wu, R. J., Peng, Y., ... & Xia, J. (2024). Performance characteristics of micro fiber-reinforced ambient cured one-part geopolymer mortar for repairing. Construction and Building Materials, 415, 135086. doi:10.1016/j.conbuildmat.2024.135086.

[22] Shamsah, M., Kalfat, R., & Subramaniam, K. V. L. (2025). Impact of low NaOH molarities on mechanical and durability properties of ambient and oven-cured fly ash geopolymer concrete. Journal of Building Engineering, 105, 112491. doi:10.1016/j.jobe.2025.112491.

[23] Wu, H., He, M., Wu, S., Cheng, J., Wang, T., Che, Y., Du, Y., & Deng, Q. (2024). Effects of binder component and curing regime on compressive strength, capillary water absorption, shrinkage and pore structure of geopolymer mortars. Construction and Building Materials, 442, 137707. doi:10.1016/j.conbuildmat.2024.137707.

[24] Trincal, V., Multon, S., Benavent, V., Lahalle, H., Balsamo, B., Caron, A., Bucher, R., Diaz Caselles, L., & Cyr, M. (2022). Shrinkage mitigation of metakaolin-based geopolymer activated by sodium silicate solution. Cement and Concrete Research, 162, 106993. doi:10.1016/j.cemconres.2022.106993.

[25] İlcan, H., Demirbaş, A. O., Ulugöl, H., & Şahmaran, M. (2024). Low-alkaline activated construction and demolition waste-based geopolymers. Construction and Building Materials, 411, 134546. doi:10.1016/j.conbuildmat.2023.134546.

[26] Chen, M., Wu, D., Chen, K., Liu, C., Zhou, G., & Cheng, P. (2025). The effects of solid activator dosage and the liquid-solid ratio on the properties of FA-GGBS based one-part geopolymer. Construction and Building Materials, 463, 140067. doi:10.1016/j.conbuildmat.2025.140067.

[27] de Klerk, D., Naghizadeh, A., Ekolu, S. O., & Welman-Purchase, M. (2025). Recycled cement use to produce fly ash – based geopolymer binders suitable for ambient curing: Comparison with slag effects. Construction and Building Materials, 468, 140394. doi:10.1016/j.conbuildmat.2025.140394.

[28] Yan, G., Hu, J., Chen, M., Ma, Y., Huang, H., Zhang, Z., Wei, J., Shi, C., & Yu, Q. (2025). Performance evaluation of reinforced slag-fly ash-ceramic waste powders ternary geopolymer concrete under chloride ingress environment. Construction and Building Materials, 478, 141447. doi:10.1016/j.conbuildmat.2025.141447.

[29] Castel, A., Foster, S. J., Ng, T., Sanjayan, J. G., & Gilbert, R. I. (2016). Creep and drying shrinkage of a blended slag and low calcium fly ash geopolymer Concrete. Materials and Structures/Materiaux et Constructions, 49(5), 1619–1628. doi:10.1617/s11527-015-0599-1.

[30] Aldawsari, S., Kampmann, R., Harnisch, J., & Rohde, C. (2022). Setting Time, Microstructure, and Durability Properties of Low Calcium Fly Ash/Slag Geopolymer: A Review. Materials, 15(3), 876. doi:10.3390/ma15030876.

[31] Kashani, A., Provis, J. L., & Van Deventer, J. S. J. (2013). Effect of ground granulated blast furnace slag particle size distribution on paste rheology: A preliminary model. AIP Conference Proceedings, 1542(1), 1094–1097. doi:10.1063/1.4812126.

[32] Yılmaz, A., Degirmenci, F. N., & Aygörmez, Y. (2024). Effect of initial curing conditions on the durability performance of low-calcium fly ash-based geopolymer mortars. Boletin de La Sociedad Espanola de Ceramica y Vidrio, 63(4), 238–254. doi:10.1016/j.bsecv.2023.10.006.

[33] Xu, Z., Zhang, J., Zhang, J., Deng, Q., Xue, Z., Huang, G., & Huang, X. (2024). Influence of steel slag and steel fiber on the mechanical properties, durability, and life cycle assessment of ultra-high performance geopolymer concrete. Construction and Building Materials, 441, 137590. doi:10.1016/j.conbuildmat.2024.137590.

[34] Wongpattanawut, W., & Ayudhya, B. I. N. (2023). Effect of Curing Temperature on Mechanical Properties of Sanitary Ware Porcelain based Geopolymer Mortar. Civil Engineering Journal, 9(8), 1808–1827. doi:10.28991/CEJ-2023-09-08-01.

[35] Wongpattanawut, W., & Ayudhya, B. I. N. (2024). Optimizing Alkali-Concentration on Fresh and Durability Properties of Defected Sanitary Ware Porcelain based Geopolymer Concrete. Civil Engineering Journal, 10(4), 1069–1092. doi:10.28991/CEJ-2024-010-04-05.

[36] Klingsad, R., & Ayudhya, B. I. N. (2025). Shrinkage Characteristics and Abrasion Resistance of Porcelain Waste-Based Geopolymers Mortar Under Chemical Exposure. Civil Engineering Journal, 11(11), 4655–4676. doi:10.28991/CEJ-2025-011-11-012.

[37] ASTM International. (2021). ASTM C191-21: Standard Test Methods for Time of Setting of Hydraulic Cement by Vicat Needle. West Conshohocken, PA, USA. doi:10.1520/C0191-21.

[38] ASTM International. (2018). ASTM C0596-18.2: Standard Test Method for Drying Shrinkage of Mortar Containing Hydraulic Cement. West Conshohocken, PA, USA. doi:10.1520/C0596-18.2

[39] ASTM International. (2019). ASTM C1698-19: Standard Test Method for Autogenous Strain of Cement Paste and Mortar. American Society for Testing and Materials: West Conshohocken, PA, USA.

[40] ASTM International. (2012). ASTM C143/C143M-12: Standard Test Method for Slump of Hydraulic-Cement Concrete. ASTM International: West Conshohocken, PA, USA. doi:10.1520/C0143_C0143M-12.

[41] BS EN 12350-3-2009 Part 3 (2009). Vebe test, Testing fresh concrete, Concrete and concrete products. British Standard: London, UK, 9 pages,

[42] ASTM International. (1997). ASTM Standard C642: Standard Test Method for Density, Absorption, and Voids in Hardened Concrete. ASTM International: West Conshohocken, PA, USA. doi:10.1520/C0642-97.

[43] ASTM International. (2016). ASTM C109/C109M-16a: Standard Test Method for Compressive Strength of Hydraulic Cement Mortars. ASTM International: West Conshohocken, PA, USA.

[44] ASTM International. (2004). ASTM C496-96: Standard test method for splitting tensile strength of cylindrical concrete specimens. ASTM International: West Conshohocken, PA, USA.

[45] Pangdaeng, S., Phoo-ngernkham, T., Sata, V., & Chindaprasirt, P. (2014). Influence of curing conditions on properties of high calcium fly ash geopolymer containing Portland cement as additive. Materials and Design, 53, 269–274. doi:10.1016/j.matdes.2013.07.018.

[46] Punurai, W., Kroehong, W., Saptamongkol, A., & Chindaprasirt, P. (2018). Mechanical properties, microstructure and drying shrinkage of hybrid fly ash-basalt fiber geopolymer paste. Construction and Building Materials, 186, 62–70. doi:10.1016/j.conbuildmat.2018.07.115.

[47] Lee, N. K., & Lee, H. K. (2015). Reactivity and reaction products of alkali-activated, fly ash/slag paste. Construction and Building Materials, 81, 303–312. doi:10.1016/j.conbuildmat.2015.02.022.

[48] Guo, X., Shi, H., & Wei, X. (2017). Pore properties, inner chemical environment, and microstructure of nano-modified CFA-WBP (class C fly ash-waste brick powder) based geopolymers. Cement and Concrete Composites, 79, 53–61. doi:10.1016/j.cemconcomp.2017.01.007.

[49] Sathonsaowaphak, A., Chindaprasirt, P., & Pimraksa, K. (2009). Workability and strength of lignite bottom ash geopolymer mortar. Journal of Hazardous Materials, 168(1), 44–50. doi:10.1016/j.jhazmat.2009.01.120.

[50] Hannawi, K., Bian, H., Prince-Agbodjan, W., & Raghavan, B. (2016). Effect of different types of fibers on the microstructure and the mechanical behavior of ultra-high performance fiber-reinforced concretes. Composites Part B: Engineering, 86, 214-220. doi:10.1016/j.compositesb.2015.09.059.

[51] Jabbar, A. M., Hamood, M. J., & Mohammed, D. H. (2021). The effect of using basalt fibers compared to steel fibers on the shear behavior of ultra-high performance concrete T-beam. Case Studies in Construction Materials, 15, e00702. doi:10.1016/j.cscm.2021.e00702.

[52] Hanumananaik, M., & Subramaniam, K. V. L. (2023). Influence of Process Variables on Shrinkage in Low-Calcium Fly-Ash Geopolymers. Journal of Materials in Civil Engineering, 35(6), 1–10. doi:10.1061/jmcee7.mteng-14761.

[53] Ma, Y., & Ye, G. (2015). The shrinkage of alkali activated fly ash. Cement and Concrete Research, 68, 75–82. doi:10.1016/j.cemconres.2014.10.024.

[54] Ling, Y., Wang, K., & Fu, C. (2019). Shrinkage behavior of fly ash based geopolymer pastes with and without shrinkage reducing admixture. Cement and Concrete Composites, 98, 74-82. doi:10.1016/j.cemconcomp.2019.02.007.

[55] Hojati, M., & Radlińska, A. (2017). Shrinkage and strength development of alkali-activated fly ash-slag binary cements. Construction and Building Materials, 150, 808–816. doi:10.1016/j.conbuildmat.2017.06.040.

[56] Li, Z., Lu, T., Liang, X., Dong, H., & Ye, G. (2020). Mechanisms of autogenous shrinkage of alkali-activated slag and fly ash pastes. Cement and Concrete Research, 135. doi:10.1016/j.cemconres.2020.106107.

[57] Amran, M., Al-Fakih, A., Chu, S. H., Fediuk, R., Haruna, S., Azevedo, A., & Vatin, N. (2021). Long-term durability properties of geopolymer concrete: An in-depth review. Case Studies in Construction Materials, 15, 661. doi:10.1016/j.cscm.2021.e00661.

[58] Bakharev, T., Sanjayan, J. G., & Cheng, Y. B. (1999). Effect of elevated temperature curing on properties of alkali-activated slag concrete. Cement and Concrete Research, 29(10), 1619–1625. doi:10.1016/S0008-8846(99)00143-X.

[59] Ye, H., & Radlinska, A. (2017). Shrinkage mitigation strategies in alkali-activated slag, Cement and Concrete Research. 101, 131–143. doi:10.1016/j.cemconres.2017.08.025.

[60] Wongsa, A., Boonserm, K., Waisurasingha, C., Sata, V., & Chindaprasirt, P. (2017). Use of municipal solid waste incinerator (MSWI) bottom ash in high calcium fly ash geopolymer matrix. Journal of Cleaner Production, 148, 49–59. doi:10.1016/j.jclepro.2017.01.147.

[61] Rudić, O., Grengg, C., Seyrek, Y., Steindl, F., Müller, B., Zögl, I., Wohlmuth, D., Ukrainczyk, N., & Mittermayr, F. (2025). Drying shrinkage and carbonation of steel slag-metakaolin alkali-activated composites: Effect of vegetable oil addition and slag aggregates. Cement and Concrete Research, 189, 107764. doi:10.1016/j.cemconres.2024.107764.

[62] Ye, G., Lura, P., & Van Breugel, K. (2006). Modelling of water permeability in cementitious materials. Materials and Structures/Materiaux et Constructions, 39(9), 877–885. doi:10.1617/s11527-006-9138-4.

[63] Udhaya Kumar, T., Vinod Kumar, M., Lakkaboyana, S. K., Trilaksana, H., & Ansari, A. (2025). Investigation of bond strength and flexural behaviour of geopolymer aggregate concrete beams. Case Studies in Construction Materials, 22. doi:10.1016/j.cscm.2025.e04916.

[64] Tahwia, A. M., Heniegal, A. M., Abdellatief, M., Tayeh, B. A., & Elrahman, M. A. (2022). Properties of ultra-high performance geopolymer concrete incorporating recycled waste glass. Case Studies in Construction Materials, 17, 1393. doi:10.1016/j.cscm.2022.e01393.

[65] Xu, H., & Van Deventer, J. S. J. (2000). The geopolymerisation of alumino-silicate minerals. International Journal of Mineral Processing, 59(3), 247–266. doi:10.1016/S0301-7516(99)00074-5.

[66] Parthiban, K., & Saravana Raja Mohan, K., (2017). Influence of recycled concrete aggregates on the engineering and durability properties of alkali activated slag concrete, Construction and Building Materials, 133: 65–72. doi:10.1016/j.conbuildmat.2016.12.050.

[67] Saloni, Parveen, Lim, Y. Y., Pham, T. M. (2021). Effective utilisation of ultrafine slag to improve mechanical and durability properties of recycled aggregates geopolymer concrete, Cleaner Engineering and Technology, 5, 100330. doi:10.1016/j.clet.2021.100330.

[68] Hu, Y., Tang, Z., Li, W., Li, Y., & Tam, V. W. Y. (2019). Physical-mechanical properties of fly ash/GGBFS geopolymer composites with recycled aggregates. Construction and Building Materials, 226, 139–151. doi:10.1016/j.conbuildmat.2019.07.211.

[69] Zuaiter, M., El-Hassan, H., El-Maaddawy, T., & El-Ariss, B. (2022). Properties of Slag-Fly Ash Blended Geopolymer Concrete Reinforced with Hybrid Glass Fibers. Buildings, 12(8), 1114. doi:10.3390/buildings12081114.

[70] Posi, P., Ridtirud, C., Ekvong, C., Chammanee, D., Janthowong, K., & Chindaprasirt, P. (2015). Properties of lightweight high calcium fly ash geopolymer concretes containing recycled packaging foam. Construction and Building Materials, 94, 408–413. doi:10.1016/j.conbuildmat.2015.07.080.

[71] Ye, G., Lura, P., & Van Breugel, K. (2006). Modelling of water permeability in cementitious materials. Materials and Structures/Materiaux et Constructions, 39(9), 877–885. doi:10.1617/s11527-006-9138-4.

[72] Jennings, H. M. (2000). Model for the microstructure of calcium silicate hydrate in cement paste. Cement and Concrete Research, 30(1), 101–116. doi:10.1016/S0008-8846(99)00209-4.

[73] Palmer, M. L., Claflin, D. R., Faulkner, J. A., & Panchangam, A. (2011). Non-uniform distribution of strain during stretch of relaxed skeletal muscle fibers from rat soleus muscle. Journal of muscle research and cell motility, 32(1), 39-48. doi:10.1007/s10974-011-9250-0.

[74] Rajak, M., & Rai, B. (2019). Effect of Micro Polypropylene Fibre on the Performance of Fly Ash-Based Geopolymer Concrete. Journal of Applied Engineering Sciences, 9(1), 97–108. doi:10.2478/jaes-2019-0013.

[75] Awwad, E., Mabsout, M., Hamad, B., Farran, M. T., & Khatib, H. (2012). Studies on fiber-reinforced concrete using industrial hemp fibers. Construction and Building Materials, 35, 710–717. doi:10.1016/j.conbuildmat.2012.04.119.

[76] Naraganti, S. R., Pannem, R. M. R., & Putta, J. (2019). Impact resistance of hybrid fibre reinforced concrete containing sisal fibres. Ain Shams Engineering Journal, 10(2), 297–305. doi:10.1016/j.asej.2018.12.004.

[77] Chen, S., Ruan, S., Zeng, Q., Liu, Y., Zhang, M., Tian, Y., & Yan, D. (2022). Pore structure of geopolymer materials and its correlations to engineering properties: A review. Construction and Building Materials, 328. doi:10.1016/j.conbuildmat.2022.127064.

[78] Farhana, Z. F., Kamarudin, H., Rahmat, A., & Bakri, A. M. M. Al. (2014). A study on relationship between porosity and compressive strength for geopolymer paste. Key Engineering Materials, 594–595, 1112–1116. doi:10.4028/www.scientific.net/KEM.594-595.1112.

[79] ACI Committee. (1999). Building code requirements for structural concrete: (ACI 318-99); and commentary (ACI 318R-99). American Concrete Institute, Farmington Hills, Michigan, USA.

[80] ACI Committee. (1992). State-of-the-Art Report on High-Strength Concrete: (ACI 363R-92). American Concrete Institute, Farmington Hills, Michigan, USA.

[81] Raphael, J. M. (1984). Tensile Strength of Concrete. Journal of the American Concrete Institute, 81(2), 158–165. doi:10.1007/978-3-642-41714-6_200519

[82] Lavanya, G., & Jegan, J. (2015). Evaluation of relationship between split tensile strength and compressive strength for geopolymer concrete of varying grades and molarity. International Journal of Applied Engineering Research, 10(15), 35523–35529.

[83] Arioglu, N., Canan Girgin, Z., & Arioglu, E. (2006). Evaluation of ratio between splitting tensile strength and compressive strength for concretes up to 120 MPa and its application in strength criterion. ACI Materials Journal, 103(1), 18–24. doi:10.14359/15123.

[84] Khoso, S., Raad, J., & Parvin, A. (2019). Experimental Investigation on the Properties of Recycled Concrete Using Hybrid Fibers. Open Journal of Composite Materials, 09(02), 183–196. doi:10.4236/ojcm.2019.92009.